


RESEARCH

Open Access



# MSC–extracellular vesicle microRNAs target host cell-entry receptors in COVID-19: in silico modeling for in vivo validation

Hajer A. Al Saihati<sup>1\*</sup>, Arigue A. Dessouky<sup>2</sup>, Rabab F. Salim<sup>3</sup>, Islam Elgohary<sup>4</sup>, Mohamed El-Sherbiny<sup>5,6</sup>, Fares E. M. Ali<sup>7</sup>, Mahmoud M. A. Moustafa<sup>8</sup>, Dalia Shaheen<sup>9</sup>, Nicholas Robert Forsyth<sup>10,14</sup>, Omnia A. Badr<sup>8\*</sup>  and Nesrine Ebrahim<sup>11,12,13,14\*</sup>

## Abstract

**Background** Coronavirus disease 2019 (COVID-19) has created a global pandemic with significant morbidity and mortality. SARS-CoV-2 primarily infects the lungs and is associated with various organ complications. Therapeutic approaches to combat COVID-19, including convalescent plasma and vaccination, have been developed. However, the high mutation rate of SARS-CoV-2 and its ability to inhibit host T-cell activity pose challenges for effective treatment. Mesenchymal stem cells (MSCs) and their extracellular vesicles (MSCs–EVs) have shown promise in COVID-19 therapy because of their immunomodulatory and regenerative properties. MicroRNAs (miRNAs) play crucial regulatory roles in various biological processes and can be manipulated for therapeutic purposes.

**Objective** We aimed to investigate the role of lyophilized MSC–EVs and their microRNAs in targeting the receptors involved in SARS-CoV-2 entry into host cells as a strategy to limit infection. In silico microRNA prediction, structural predictions of the microRNA–mRNA duplex, and molecular docking with the ArgonAUT protein were performed.

**Methods** Male Syrian hamsters infected with SARS-CoV-2 were treated with human Wharton's jelly-derived Mesenchymal Stem cell-derived lyophilized exosomes (Biologica Company) via intraperitoneal injection, and viral shedding was assessed. The potential therapeutic effects of MSCs–EVs were measured via histopathology of lung tissues and PCR for microRNAs.

**Results** The results revealed strong binding potential between miRNA–mRNA duplexes and the AGO protein via molecular docking. MSCs–EVs reduced inflammation markers and normalized blood indices via the suppression of viral entry by regulating ACE2 and TMPRSS2 expression. MSCs–EVs alleviated histopathological aberrations. They improved lung histology and reduced collagen fiber deposition in infected lungs.

**Conclusion** We demonstrated that MSCs–EVs are a potential therapeutic option for treating COVID-19 by preventing viral entry into host cells.

**Keywords** COVID-19, MSC–EVs, MicroRNAs, Receptors for viral entry, Molecular docking

\*Correspondence:

Hajer A. Al Saihati

hajirsh@uhb.edu.sa

Omnia A. Badr

omnia.badr@fagr.bu.edu.eg

Nesrine Ebrahim

Nesrien.salem@fmed.bu.edu.eg; n.i.a.hussein@keele.ac.uk

Full list of author information is available at the end of the article



© The Author(s) 2024. **Open Access** This article is licensed under a Creative Commons Attribution-NonCommercial-NoDerivatives 4.0 International License, which permits any non-commercial use, sharing, distribution and reproduction in any medium or format, as long as you give appropriate credit to the original author(s) and the source, provide a link to the Creative Commons licence, and indicate if you modified the licensed material. You do not have permission under this licence to share adapted material derived from this article or parts of it. The images or other third party material in this article are included in the article's Creative Commons licence, unless indicated otherwise in a credit line to the material. If material is not included in the article's Creative Commons licence and your intended use is not permitted by statutory regulation or exceeds the permitted use, you will need to obtain permission directly from the copyright holder. To view a copy of this licence, visit <http://creativecommons.org/licenses/by-nc-nd/4.0/>.

## Introduction

Severe acute respiratory syndrome coronavirus 2 (SARS-CoV-2), which causes coronavirus disease 2019 (COVID-19), was initially identified in Wuhan, China, in December 2019 [1]. The World Health Organization named COVID-19 an international public health emergency on January 30, 2020, and a global pandemic on March 11, 2020 [2]. The COVID-19 outbreak developed into a protracted international health emergency. As of 21 March 2023, there were over 761,071,826 unique coronavirus infections worldwide, with over 6,879,677 fatalities and over 88,298,471 recoveries [3]. SARS-CoV-2 is a member of the coronavirus (CoV) family of viruses, a broad group of potentially deadly RNA viruses that are frequently linked to respiratory illnesses. The lungs are the predominant location of SARS-CoV-2 infection in humans, but infection can adversely affect other organs. Fever, dry cough, and exhaustion are the main signs of COVID-19 following a SARS-CoV-2 incubation period that lasts approximately 14 days [4].

SARS-CoV-2 is a positive-sense, single-stranded RNA virus with a spherical envelope that typically ranges in size from 80 to 120 nm. It belongs to the genus Betacoronavirus. The genome of SARS-CoV-2 contains instructions for the synthesis of various proteins, both structural and nonstructural. Among these proteins, the spike (S), nucleocapsid (N), membrane (M), and envelope (E) proteins play critical roles in the life cycle of the virus. The S protein is further divided into S1 and S2 subunits. The S1 subunit facilitates the attachment of the virus to host cells through its interaction with ACE2 receptors, whereas the S2 subunit promotes the fusion of the viral and host cell membranes. The presence of specific amino acids, including glutamine, asparagine, leucine, phenylalanine, and serine, in the spike protein of SARS-CoV-2 enhances its affinity for ACE2 receptors, thereby assisting in viral attachment [4]. Moreover, proteases originating from the host, such as TMPRSS2 and endosomal cysteine proteases, cleave the S protein of SARS-CoV-2, leading to the activation of the virus and its binding to the ACE2 receptor on human cell surfaces. This activation process results in the release of the virus's genetic material into the host cell, followed by the fusion of the viral envelope and the cell membrane. By imposing stricter restrictions on these host targets, it may be possible to impede the entry of SARS-CoV-2 into cells and mitigate the development of illness [5, 6].

To combat the morbidity and mortality associated with COVID-19, numerous therapeutic approaches have been developed [7]. Convalescent plasma and vaccination may both be effective forms of treatment, but only if stable viral epitopes are present. SARS-CoV-2 has a high mutation rate and can directly inhibit host T-cell activity,

making treatments ineffective [8]. For COVID-19 therapy, mesenchymal stem cells (MSCs) and extracellular vesicles produced from MSCs may be helpful. Extracellular vesicles are superior to parental MSCs in terms of their ease of handling in clinical settings [9]. Extracellular vesicles are a useful strategy for antiviral treatments, including COVID-19 [10], owing to their inherent qualities in connection with immunomodulation, wound healing, and drug delivery. Proteins, messenger RNAs (mRNAs), small and long noncoding RNAs (ncRNAs), DNA, lipids, and carbohydrates from the parental MSCs are carried within the lipidic bilayer of extracellular vesicles and can alter the behavior of target cells with angiogenic, immunomodulatory, and regenerative effects [11].

MicroRNAs (miRNAs) are small, highly conserved, noncoding single-stranded ribonucleic acids (RNAs) that bind to the 3'-untranslated regions (UTRs) of target mRNAs to promote messenger RNA (mRNA) degradation and/or impede protein translation [12, 13]. They have been thoroughly studied in cardiovascular medicine and serve crucial regulatory functions in many biological processes, both in health and in disease [14–16]. Since their activity can be effectively controlled by cutting-edge RNA-based technologies, the use of miRNAs constitutes a particularly alluring technique to manipulate numerous processes in terms of their therapeutic potential [17, 18].

The main aim of this study was to investigate whether lyophilized MSC-EVs have inhibitory effects on SARS-CoV-2 infection both *in silico* and *in vivo*. This study aimed to utilize computational analysis to assess the binding affinity of specific miRNAs contained in MSC-EVs with relevant receptors, indicating their potential as therapeutic targets for combating SARS-CoV-2 infection. Additionally, *in vivo* experiments were conducted to examine the ability of lyophilized MSC-EVs to modulate the expression of miRNAs, ACE2 and TMPRSS2 receptors, as well as viral protein expression, to prevent SARS-CoV-2 from entering host cells. This study sought to elucidate the inhibitory mechanisms of MSCs-EVs on SARS-CoV-2 through both computational and experimental approaches, providing valuable insights for the development of effective therapeutic interventions.

## Materials and methods

### *In silico* study

#### *MicroRNA prediction*

The SARS-CoV-2 entry receptors ACE2, TMPRSS2, ITGA3, ITGA5, ITGAV, and CTS1 were used to identify and correlate interacting microRNAs via miRTarBase (<http://mirtarbase.mbc.nctu.edu.tw/php/index.php>). The expression of 10 miRNAs (miR-200c-3p, miR-26b-5p, miR-125b-5p, miR-98-5p, miR-214-3p, miR-32-3p, miR-98-3p, miR-92a-3p, miR-32-5p, and miR-31-5p) in MSC-derived

extracellular vesicles (MSCs–EVs) via EVmiRNA interrogation (<http://bioinfo.life.hust.edu.cn/EVmiRNA#!/>) and ExoCarta (<http://www.exocarta.org/>) revealed microRNA–target interactions with these receptors. A literature analysis revealed five additional miRNA-derived MSC–EVs (miR-30a-5p, miR-17-5p, miR-27b-3p, miR-143-3p, and let-7f-5p) with the potential to interact with the ACE2, TMPRESS2 and CSTL1 receptors [19, 20]. To identify the interacting sequence positions of these receptors with the predicted miRNAs, pairwise sequence alignment between the predicted microRNA and the 3'UTR of the target receptor was performed via BLASTN.

#### **Structural prediction of microRNAs–mRNA duplex**

Duplex sequences of microRNA–receptor mRNAs were used as inputs for the RNA fold (<http://rna.tbi.univie.ac.at/cgi-bin/RNAWebSuite/RNAfold.cgi>) for prediction of the duplex secondary structure of microRNA–mRNA and the dot-bracket notation of both. The 3-dimensional structure of each duplex was predicted via RNA-COMPOSER (<https://rnacomposer.cs.put.poznan.pl>).

#### **Molecular docking of duplexes with argonaut protein**

The protein component of the RNA-induced silencing complex (RISC) is the argonaut protein (AGO). The PDB format of the argonaut silencing complex was retrieved with the ID 3F73 (<https://www.rcsb.org/>). Protein preparation for this complex was performed according to Fadaka et al. [21]. The PDB files of the microRNAs, microRNA–mRNAs, and AGO proteins were submitted to PATCHDOCK (<https://bioinfo3d.cs.tau.ac.il/PatchDock/php/>). The shape complementarity theory is the basis of the PatchDock approach [22], and its applicability in molecular docking studies has been described elsewhere [23]. PATCHDOCK was employed for molecular docking analysis between chain A of the AGO protein and the microRNA–mRNA duplex. The clustering root-mean-square deviation (RMSD) was selected as 2.0 Å for the protein–small ligand complex type. The highest pose score was considered to be the best complex [23]. For visualization of the results, the Biovia Discovery Studio Viewer 2021 (Biovia DSV 2021) was used to present interactions, including receptor surface interactions (hydrogen bonding and charging) in the docked conformations and the surface interactions of the microRNA–mRNA–AGO complex.

**In vivo study (this work has been reported in line with the ARRIVE guidelines for stem cell research and therapy)**

#### **Experimental animals**

Male adult Syrian hamsters, 100–150 g in weight, were sourced from the National Research Centre (NRC), Egypt. The animals were maintained in tidy cages with

free access to clean drinking water and normal rodent feed. The animals were familiarized with an environment that featured daylight cycling (12-h cycles beginning at 8:00 AM) and room temperature (23 °C). The animals were handled in accordance with international and national ethical standards.

This study was performed under NRC's ethical committee approval (approval number: NRC-20074), and all procedures and experiments were carried out per the approval. In controlled laboratory and biosafety circumstances, live viral infection studies were conducted in negative pressure-based level 3 isolators (PLAS LABS, Lansing, MI). Additionally, all of the experimental procedures adhered to the guidelines and approval of the institutional review board (BUFVTM 13-04-22, Faculty of Veterinary Medicine, Benha University, Egypt). The National Institutes of Health Guide for the Care and Use of Laboratory Animals (NIH publication 85-23, revised 2011) was strictly followed in all experiments.

#### **Virus and cells**

The SARS-CoV-2 virus strain hCoV-19/Egypt/NRC-03/2020 was propagated in Vero E6 cells (ATCC No. CRL-1586) at an MOI of 0.005, maintained at 37 °C in 5% CO<sub>2</sub> in a humid incubator, and observed microscopically daily. GISAID accession number: EPI\_ISL\_430819 was applied to this sample. At 72 h post infection, the virus-infected culture supernatant was removed, clarified by centrifugation twice for 15 min at 4 °C, aliquoted and titrated via a plaque assay [24]. Briefly, the virus was utilized to infect Vero-E6 cells in a 6-well cell culture plate and was serially diluted ten times in cell maintenance media before being incubated for an hour at 37 °C with 5% CO<sub>2</sub>. The cell controls were noninfected wells. The plates were cultured for 72 h at 37 °C with 5% CO<sub>2</sub> after infection, after which 3 ml of overlay medium with agarose was added and held at room temperature for solidification. Fixation and virus inactivation were carried out using a (10%) formalin solution for 1 h. Following fixation, the overlay was removed, and a 0.1% crystal violet solution was applied for staining. Plaque-forming units (PFUs)/ml = number of plaques × virus-injected volume × viral dilution × 10 was used for viral titer determination.

#### **MSCs–extracellular vesicles (MSCs–EVs)**

**Source of lyophilized MSCs–EVs** Human Wharton's jelly-derived Mesenchymal Stem cell-derived lyophilized exosomes were purchased from Bioluga® (Canada) with Certificate ID: TU35-5ZN4. The EVs were reconstituted in 5 ml distilled water, where 1 ml contained MSC–EVs derived from  $0.5 \times 10^6$  MSCs [25, 26]. Lyophilization process as stated in the COA of the product was by freeze

drying and sublimation using a cryoprotectant stabilizer which improves its stability and temperature tolerance and increases the shelf life and extends preservation periods of exosomes without losing its intrinsic cargo or harmful effects on the exosomal membranes [25].

#### **Infection challenge of hamsters**

Viral microneutralization was used to confirm the seronegative status of the male Syrian hamsters. Ketamine–xylazine was used to anesthetize Syrian hamsters individually (K, 100 mg/kg; X, 10 mg/kg). Hamsters were intranasally challenged with 100 µL containing 50 µL of SARS-CoV-2 and observed for an additional 7 days [27]. A 0.5 ml intraperitoneal injection of MSCs–EVs was given to the corresponding group 8 h after infection.

#### **Titration of viral shedding**

A sterile 0.5 ml of 1×PBS supplemented with a 2% antibiotic antimetabolic combination was flushed through the animal's nose to collect nasal washes from infected hamsters (group II) and infected hamsters treated with MSC–EVs [28]. Two hundred microliters of each sample was subjected to total RNA extraction before being subjected to qRT–PCR to target the ORF1b–nsp14 gene, as previously described [24, 29].

#### **Viral microneutralization assay (VMN)**

As indicated above, the viral microneutralization (VMN) assay was used to confirm that the Syrian hamsters lacked anti-SARS-CoV-2 antibodies. It was also used to determine seroconversion against SARS-CoV-2 in the collected sera from treated and control infected animals, as previously described [30, 31].

Serum samples were inactivated by heating for 30 min at 56 °C and then held at 20 °C. Serum samples were prepared in twofold serial dilutions ranging from 1:10 to 1:1280 in 50 l of maintenance cell culture medium. A 100 TCID<sub>50</sub>/ml hCoV-19/Egypt/NRC-03/2020 SARS-CoV-2 isolate was produced as the virus and combined in equal parts with serially diluted serum. The mixture was aliquoted in duplicate into 96-well plates containing Vero-E6 cells and incubated for 1 h at 37 °C before being removed. Following the removal of the inoculums, maintenance DMEM containing 2% bovine serum albumin (BSA) was added. The plates were then placed in a humidified incubator for three days at 37 °C with 5% CO<sub>2</sub>. The highest serum dilution that completely neutralized the virus was recorded as the neutralizing antibody titer.

#### **Experimental design**

Following acclimatization, 28 male Syrian hamsters were randomly divided into three groups:

*Group I (control group; n=14):* The hamsters were divided equally into two subgroups:

*Subgroup Ia:* Standard laboratory conditions without any intervention.

*Subgroup Ib:* Single intraperitoneal injection with 0.5 ml of phosphate-buffered saline.

*Group II (COVID-19 group; n=7):* Hamsters were sacrificed after 7 days of infection challenge (at the end of the experiment).

*Group III (MSCs–EVs; n=7):* Eight hours after infection challenge, the hamsters were injected intraperitoneally with 0.5 ml of MSC–EVs at a single concentration (100 µg protein/ml).

The timeline of the experimental design denotes the duration of the experiment, the experimental groups and the time at which the treatments were administered (Fig. 1). Body temperature and weight were measured daily for each group, and any changes in mortality or morbidity were noted. The nasal washes of the anesthetized animals were taken at days 1, 3, 5, and 7 after infection. The viral titer in the nasal washes was determined as described above in “[Titration of viral shedding](#)” Section.

#### **Sampling**

In our animal experiments, we carried out euthanasia of the rats using a two-step procedure in full compliance with our institutional guidelines for humane animal research. First, the rats were administered an intramuscular injection of a combination of ketamine (100 mg/kg) and xylazine (10 mg/kg) to induce deep surgical anesthesia. Ketamine is a dissociative anesthetic that inhibits pain perception and produces a cataleptic state, while xylazine is an alpha-2 adrenergic agonist that provides sedation, muscle relaxation, and analgesia. This anesthetic regimen is a widely accepted and commonly used method to humanely anesthetize rodents prior to euthanasia. Once the animals were confirmed to be in a deep plane of anesthesia, as evidenced by the loss of withdrawal reflexes and lack of response to stimuli, we proceeded with euthanasia. Euthanasia was performed by exsanguination (cardiac puncture) to ensure death. This method involves the collection of a terminal blood sample via the retro-orbital sinus, which results in the rapid depletion of blood volume and death of the animal under deep anesthesia. The entire euthanasia process was carried out by trained personnel in a dedicated euthanasia room, using techniques that minimize any potential pain or distress to the animals. All procedures were reviewed and approved by our Institutional Animal Care and Use Committee (IACUC) to ensure they adhered to the highest standards of humane animal research and have been reported in line with the ARRIVE 2.0 guidelines.



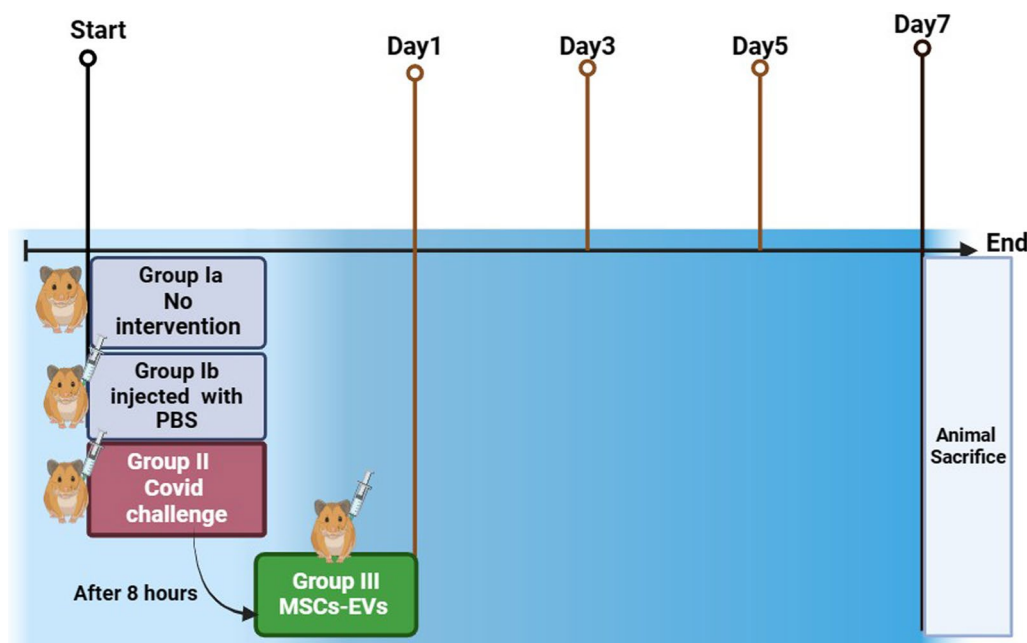


**Fig. 1** Timeline of the experimental design

Following a 7-day viral challenge, the hamsters were fasted for 12 h before being given an intramuscular injection of ketamine (100 mg/kg) and xylazine (10 mg/kg) to induce anesthesia. Using a capillary tube and retro-orbital sinus blood, total blood and serum samples were taken from the anesthetized animals before and 7 days after infection [32]. Blood samples were taken in sterile ethylenediaminetetraacetic acid (EDTA) vacutainer tubes, and all animal sera were isolated and stored at 20 °C until use. Arterial perfusion fixation was carried out through the left ventricle while the hamsters were immobilized. Three sections of lung tissues were separated. For histopathological analyses, the first component was fixed in 10% formaldehyde, cleaned, dried, and embedded in paraffin blocks. To evaluate the virus titers in each collected organ, the second half was stored in RNeasy prior to being homogenized. The third portion was set aside in SDS buffer.

#### **Complete blood count (CBC) and C-reactive protein (CRP) analyses**

Both complete blood count (CBC) and C-reactive protein (CRP) analyses were conducted instrumentally. For the CBC procedure, blood collection was conducted through retroorbital sinus puncture in an anesthetized hamster via a microhematocrit capillary tube inserted into the medial canthus of the eye to puncture the retroorbital sinus. The collected blood, which was treated with EDTA as an anticoagulant, was analyzed via an

automated hematology analyzer tailored for hamster blood. This facilitates the measurement of crucial parameters, including red and white blood cell counts, hemoglobin, hematocrit, and platelet levels. Simultaneously, for CRP analysis, blood was collected following the same method used for CBC. After collection, serum separation is achieved by allowing the blood to clot, followed by centrifugation and careful removal of the resulting supernatant. The quantification of CRP levels in the serum was subsequently accomplished via enzyme-linked immunosorbent assay (ELISA) kits specifically designed for hamsters (catalog no. MBS1604138), with adherence to the manufacturer's instructions for the assay. This dual approach provides comprehensive insight into the hematological profile and inflammatory status of rodents, which is essential for a thorough understanding of their physiological condition.

#### **Quantitative real-time PCR for miRNAs**

miRNA was isolated from lung tissue via a mirPremier microRNA Isolation Kit (Sigma–Aldrich). Following the manufacturer's instructions, cDNA was synthesized from miRNAs using an Invitrogen NCode VILO miRNA cDNA Synthesis Kit and a Bio-Rad T100 Thermal Cycler (USA) with U6 as an internal control for miRNA quantification [33]. The primer pairs used for the amplification of miR-200c-3p, miR-26b-5p, miR-125b-5p, miR-98-5p, miR-214-3p, miR-32-3p, miR-98-3p, miR-92a-3p, miR-32-5p, miR-31-5p, miR-30a-5p, miR-17-5p, miR-27b-3p,

miR-143-3p, let-7f-5p, and U6 were purchased from Genewiz (New Jersey, USA) (Table 1). For qRT–PCR, Maxima SYBR Green/ROX qPCR master mix [2x] (Thermo Scientific, USA) was utilized according to Ebrahim et al., 2022. The equation  $RQ=2^{-\Delta\Delta C_t}$  was used to calculate the relative gene expression ratios (RQs) between the treated and control groups [34].

Histopathological analysis

H&E and masson trichrome staining

Fixed lung tissue samples were used to prepare paraffin sections of 4–6 μm thickness. The sections were mounted on glass slides for subsequent staining. For H&E, increasing concentrations of ethanol were used to dehydrate the fixed sections. The dehydrated sections were then washed twice in distilled water, followed by H&E staining. Two blinded experienced investigators performed the examination, analysis, and imaging of the lung tissue sections via light microscopy (Leica DMR 3000; Leica Microsystems) [35].

Immunohistochemistry analysis

Paraffin sections were deparaffinized and hydrated. Endogenous peroxidase activity was blocked with 10% hydrogen peroxide, after which the sections were incubated with primary antibodies directed against specific targets (Anti-SARS-CoV-2 (rabbit polyclonal to SARS-CoV-2, 1/100–1/1000 concentration, ab229227, Abcam), TMPRSS2 (rabbit polyclonal to TMPRSS2, 1/100–1/500 concentration, ab214462, Abcam), and ACE2 (rabbit polyclonal to ACE2, ab15348, Abcam). Anti-CD105 (rabbit polyclonal, AA 58–110; Catalog No. ABIN707561) and

CD73 antibody (rabbit polyclonal, AA 520–550; Catalog No. ABIN388750) were used.

The slides were washed with phosphate buffer before the biotinylated goat anti-rabbit secondary antibody IgG H&L (HRP) (ab6721) was applied. For localization of the immune reaction, the slides were incubated with avidin–biotin peroxidase using diaminobenzidine as a chromogen for visualization [36]

Morphometric study

H&E, Masson’s trichrome and immunostained sections were assessed and scored by two skilled pathologists who were unaware of the experimental techniques. Morphometric measurements were carried out with at least two sections per animal using ImageJ® software version 1.52a28 and Fiji ImageJ software [37]. For each section, three distinct, nonoverlapping fields were assessed. The lung injury scoring system previously reported by Huang and Shi [38] was used to quantify the pathological injury to the lung tissue. The pathology indices included alveolar wall thickness, alveolar congestion, lung edema, hemorrhage, and infiltration of neutrophils into the airspace or vessel wall. The scoring system was as follows: lung hemorrhage (0=no hemorrhage, 1=mild hemorrhage, 2=severe hemorrhage), lung interstitial edema (0=no edema, 1=mild edema, 2=severe edema), alveolar wall thickness (0=no alveolar wall thickness, 1=mid-alveolar wall thickness, 2=severe alveolar wall thickness, and 3=severe alveolar wall thickness with > 50% lung consolidation) and infiltration of inflammatory cells (0=no inflammatory cell infiltration, 1=mild

Table 1 Sequences for primers

miRNA	Forward	Universal reverse	Accession
miR-200c-3p	GTTTGTAACTAGCCGGGTAAT	GTGCAGGGTCCGAGGT	MIMAT0000617
miR-26b-5p	GTTTGGGTCAAGTAATTCAGG	GTGCAGGGTCCGAGGT	MIMAT0000083
miR-125b-5p	GTTTCCCTGAGACCCTAAC	GTGCAGGGTCCGAGGT	MIMAT0000423
miR-98-5p	GTTTGGTGAGGTAGTAAGTTGT	GTGCAGGGTCCGAGGT	MIMAT0000096
miR-214-3p	GTTACAGCAGGCACAGACA	GTGCAGGGTCCGAGGT	MIMAT0000271
miR-32-3p	GTTTGGCAATTAGTGTGTGTG	GTGCAGGGTCCGAGGT	MIMAT0004505
miR-98-3p	GTTGGGCTATACAACCTACTAC	GTGCAGGGTCCGAGGT	MIMAT0022842
miR-92a-3p	GTGTATTGCACCTTGCCCG	GTGCAGGGTCCGAGGT	MIMAT0000092
miR-32-5p	GTGGGGTATTGCACATTACTAA	GTGCAGGGTCCGAGGT	MIMAT0000090
miR-31-5p	GTTTAGGCAAGATGCTGGC	GTGCAGGGTCCGAGGT	MIMAT0000089
miR-30a-5p	GGGTGTAAACATCCTCGAC	GTGCAGGGTCCGAGGT	MIMAT0000087
miR-17-5p	GGCAAAGTGCTTACAGTGC	GTGCAGGGTCCGAGGT	MIMAT0000070
miR-27b-3p	GTGGTTCACAGTGGCTAAG	GTGCAGGGTCCGAGGT	MIMAT0000419
miR-143-3p	GTGGTGAGATGAAGCACTG	GTGCAGGGTCCGAGGT	MIMAT0000435
let-7f-5p	GTTTGGTGAGGTAGTAGATTGT	GTGCAGGGTCCGAGGT	MIMAT0000067
U6	CTCGCTTCGGCAGCACA	AACGCTTCACGAATTTGCGT	Ebrahim et al., 2022



energy requirement for disassembling the complex atoms into free electrons. The negative binding energy values suggested that the AGO protein inhibits duplex formation. The hydrogen bonding and hydrophobic interactions of the miR-200c-3p, miR-26b-5p and miR-125b-5p duplexes (Fig. 2) and the miR-17-5p, miR-27b-3p and miR-143-3p duplexes (Fig. 3) with the mRNA of ACE2 and the binding pocket of argonaut silencing complexes revealed strong binding affinity. The miR-98-5p, miR-214-3p and miR-32-3p duplexes interacted with the mRNAs of the TMPRESS2 gene and argonaut silencing protein via a number of hydrogen bonds, as illustrated in Fig. 4. The miR-98-3p-ITGA3-AGO complex and the miR-92a-3p and miR-31-5p-ITGA5-AGO complexes are illustrated in Fig. 5. Confirming the above findings, miR-32-5p bound to ITGAV mRNA, miR-30a-5p bound to CTSL1 mRNA and let-7f-5p bound with TMPRESS2 mRNA (Fig. 6). The identification of strongly hydrophobic amino acids, amino acids with aromatic side chains, and amino acids with hydrogen bonds all support the concept that microRNAs are a component of argonaut protein-mediated gene regulation.

#### MSCs-EVs do not affect viral shedding in SARS-CoV-2-infected animals

We examined changes in viral shedding over a period of seven days in both the COVID-19 group and the MSC-EV-treated group. Viral shedding, characterized by the release of viral particles from infected cells, is an important aspect of viral replication and transmission. By

analyzing the level of viral shedding, we aimed to assess whether MSC-EVs could exert an inhibitory effect on SARS-CoV-2 replication and reduce the overall viral load in infected animals.

Viral shedding gradually increased in both groups over the first three days. However, over the subsequent four days, we observed a gradual decrease in viral shedding without a statistically significant difference between the COVID-19 group and the MSC-EV-treated group. These findings suggest that the administration of MSC-EVs did not significantly reduce the overall level of viral shedding from infected animals (Fig. 7).

#### Localization of MSCs-EVs

Lyophilized MSCs-EVs retain typical EV structures, surface protein integrity, and deliver their cargo to targeted cells [41]. We investigated the localization of MSC-EVs in lung tissue via immunohistochemistry of CD105 and CD73, MSC-EVs markers. Compared with that in the control group or COVID-19 group, CD105 and CD73 expression were present in the MSC-EV group, indicating that the MSCs-EVs reached the lung tissues (Fig. 8).

#### MSCs-EVs inhibited systemic inflammation in SARS-CoV-2-infected animals

The effects of MSC-EVs on SARS-CoV-2-induced systemic inflammation were investigated by assessing CRP levels, WBC counts, and the neutrophil/lymphocyte ratio. As expected, SARS-CoV-2 infection caused a significant increase in the CRP level and neutrophil/lymphocyte ratio concomitant with a marked decrease in the WBC count. The administration of MSCs-EVs significantly inhibited SARS-CoV-2-induced systemic inflammation, as evidenced by the normalization of blood indices as well as CRP levels (Fig. 9).

#### MSC-EVs suppressed SARS-CoV-2 host cell entry by modulating the miRNA-regulated expression of ACE2, TMPRSS2, ITGA3, ITGA5, ITGAV and cathepsin L.

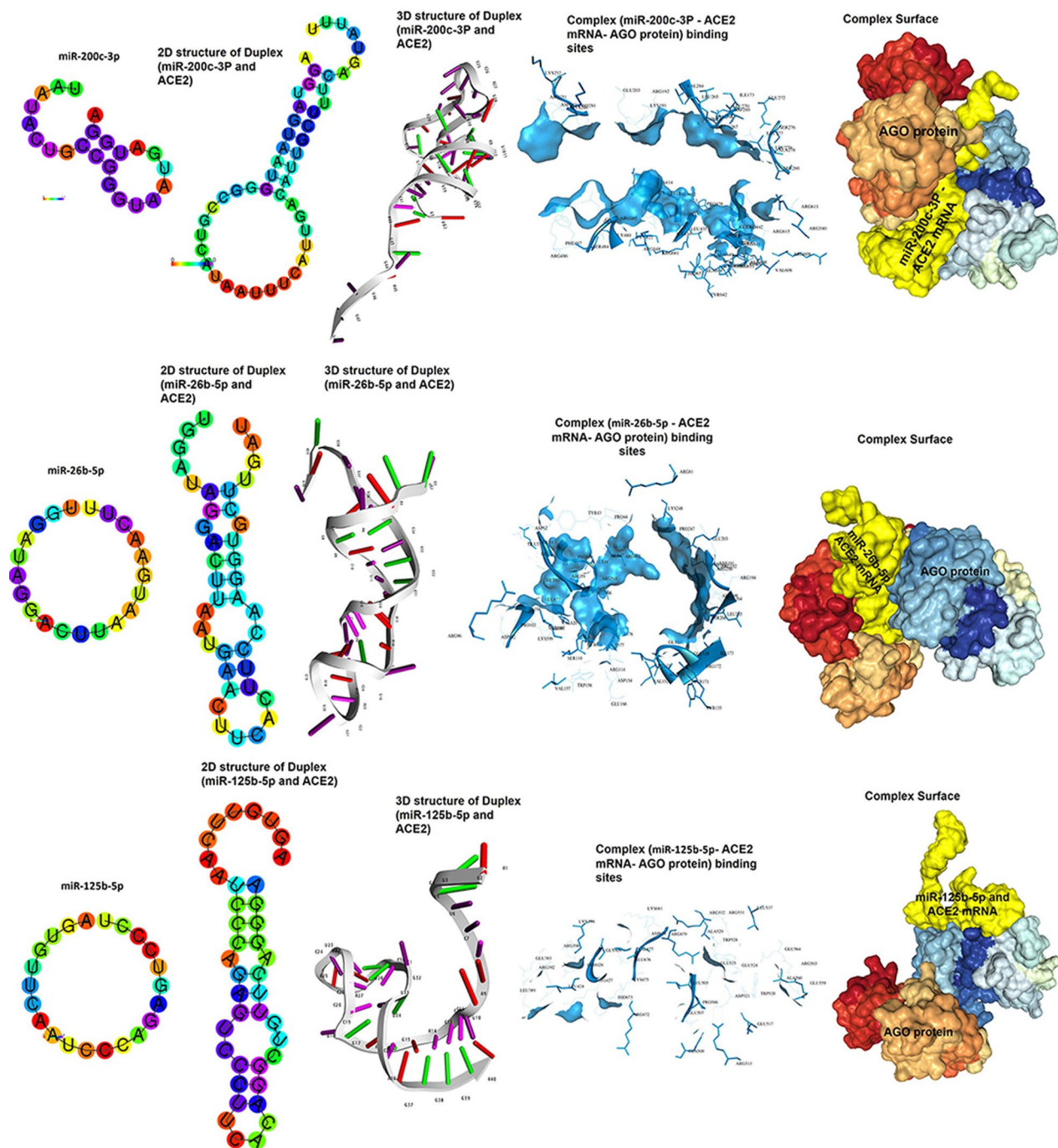
Next, we investigated the effects of MSC-EVs on the miRNAs responsible for SARS-CoV-2 entry into host lung tissue via qRT-PCR. miRNAs that target ACE2 (miR-17-5p, miR-26b-5p, miR-125b-5p, miR-143-3p, and miR-200c-3p) were significantly decreased in SARS-CoV-2-infected animals, whereas miRNAs that target ACE2 were significantly increased after MSC-EV treatment (Fig. 10A). In parallel, infection with SARS-CoV-2 caused significant upregulation of miRNAs that target TMPRSS2 (miR-98-5p, miR-214-3p, miR-32-3p and Let-7f-5P), which was consistent with the above upregulation of miR-98-5p, miR-214-3p, miR-32-3p and Let-7f-5P observed after MSC-EV treatment (Fig. 10B). On the other hand, miR-31-5p, which

**Table 3** Docking scores between miRNA-mRNA and AGO protein

miRNA-mRNA and AGO	Docking score	Area	ACE
miR-200c-3p-ACE2-AGO	23,046	4106.1	−920.02
miR-26b-5p-ACE2-AGO	23,472	4173.8	−944.68
miR-125b-5p-ACE2-AGO	20,432	2877.1	−61.04
miR-17-5p-ACE2-AGO	22,960	3556.8	−861.80
miR-27b-3p-ACE2-AGO	16,004	2939.6	−231.73
miR-143-3p-ACE2-AGO	21,118	3369.9	−594.72
miR-98-5p-TMPRSS2-AGO	19,308	2899.5	−83.25
miR-214-3p-TMPRSS2-AGO	23,308	3736.6	−783.98
miR-32-3p-TMPRSS2-AGO	23,438	3852	−877.90
let-7f-5p-TMPRSS2-AGO	21,722	3087.4	−256.60
miR-98-3p-ITGA3-AGO	21,198	3059.5	−907.88
miR-92a-3p-ITGA5-AGO	24,068	3542.4	−328.20
miR-32-5p-ITGAV-AGO	25,012	3711	−171.61
miR-31-5p-ITGA5-AGO	20,320	3160.2	−804.52
miR-30a-5p-CTSL1-AGO	21,252	3496.2	−122.26

Score indicates the geometric shape complementary score; interface area (Area); Atomic contact energy (ACE) score generated for each miRNA-mRNA and argonaute (AGO) complex





targets ITGA5, and miR-98-5p, which targets ITGA3, were significantly downregulated, whereas miR-32-5p and miR-92a-3p, which target ITGAV and ITGA5, respectively, were significantly increased in SARS-CoV-2-infected animals. MSC-EV administration resulted

in greater upregulation of integrin-targeting miRNAs, with the exception of miR-31-5p (Fig. 10C). Furthermore, the transcript level of miR-30a-5p, which targets cathepsin L, was significantly greater in SARS-CoV-2-infected animals than in normal control animals.

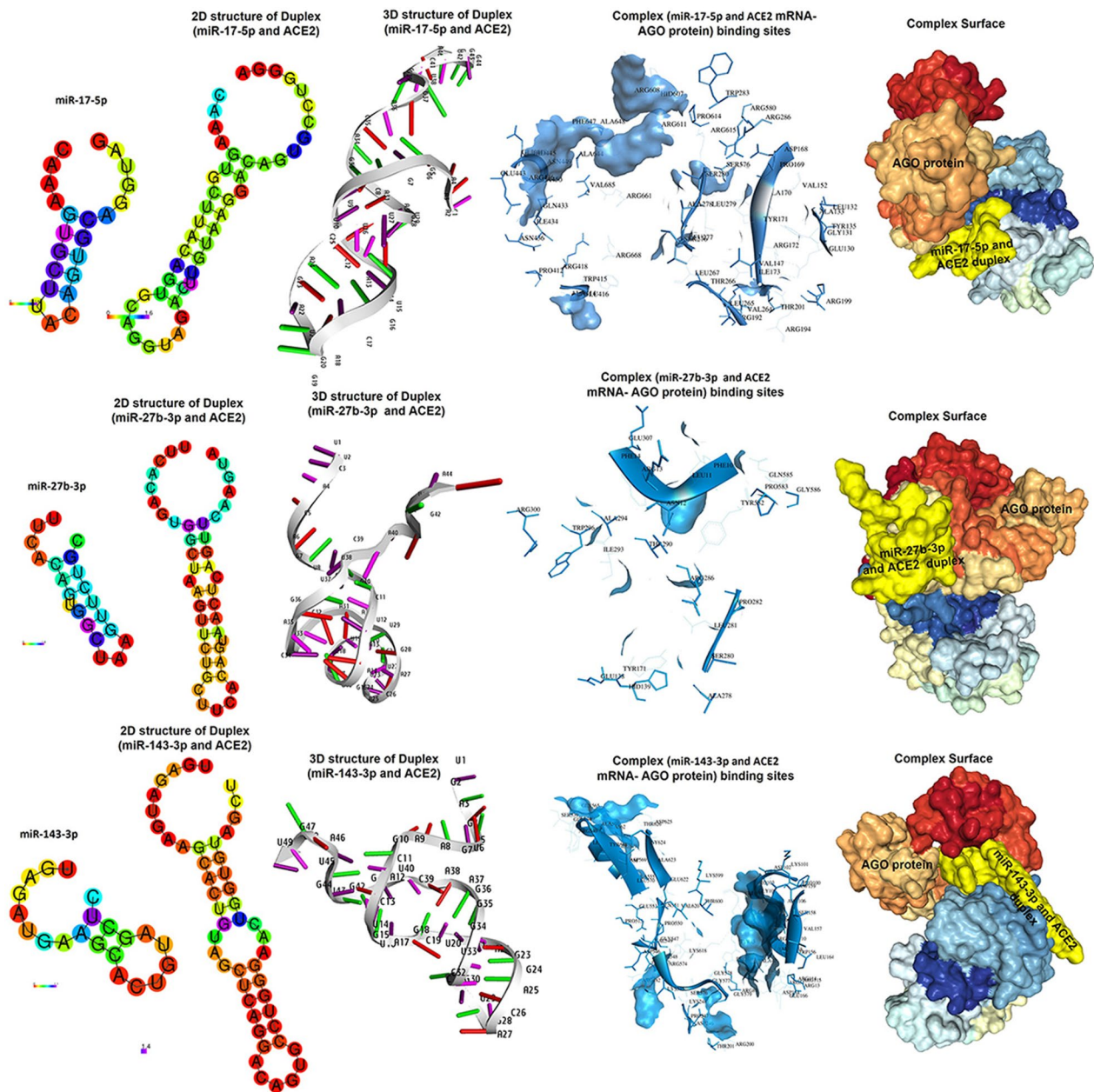


**Fig. 3** 2D structural models of miR-17-5p, miR-27b-3p and miR-143-3p; 2D and 3D structural models of different microRNAs duplexes with mRNA of ACE2 gene; Binding sites interactions between amino acid residues of Argonaute protein and microRNAs- ACE2 duplexes and surface shape of argonaute silencing complexes

Compared with those of normal and SARS-CoV-2-infected animals, the expression of miR-30a-5p increased in response to treatment with MSCs-EVs (Fig. 10D). Together, the results of the present study indicated that MSC-EV treatment prevented SARS-CoV-2 entry into host cells via the upregulation of the miRNA-related expression of ACE2, TMPRSS2, integrin, and cathepsin L.

#### MSCs-EVs downregulated TMPRSS2 and ACE2 protein expression in SARS-CoV-2-infected lung tissue

Moderate immunoreactivity for TMPRSS2 was observed in the alveolar cells of the control group (Fig. 11a). This immunoreactivity became intense and widespread across the COVID-19 infected group, with highly significant differences ( $p < 0.001$ ) compared with the control group (Fig. 11b). MSC-EV treatment



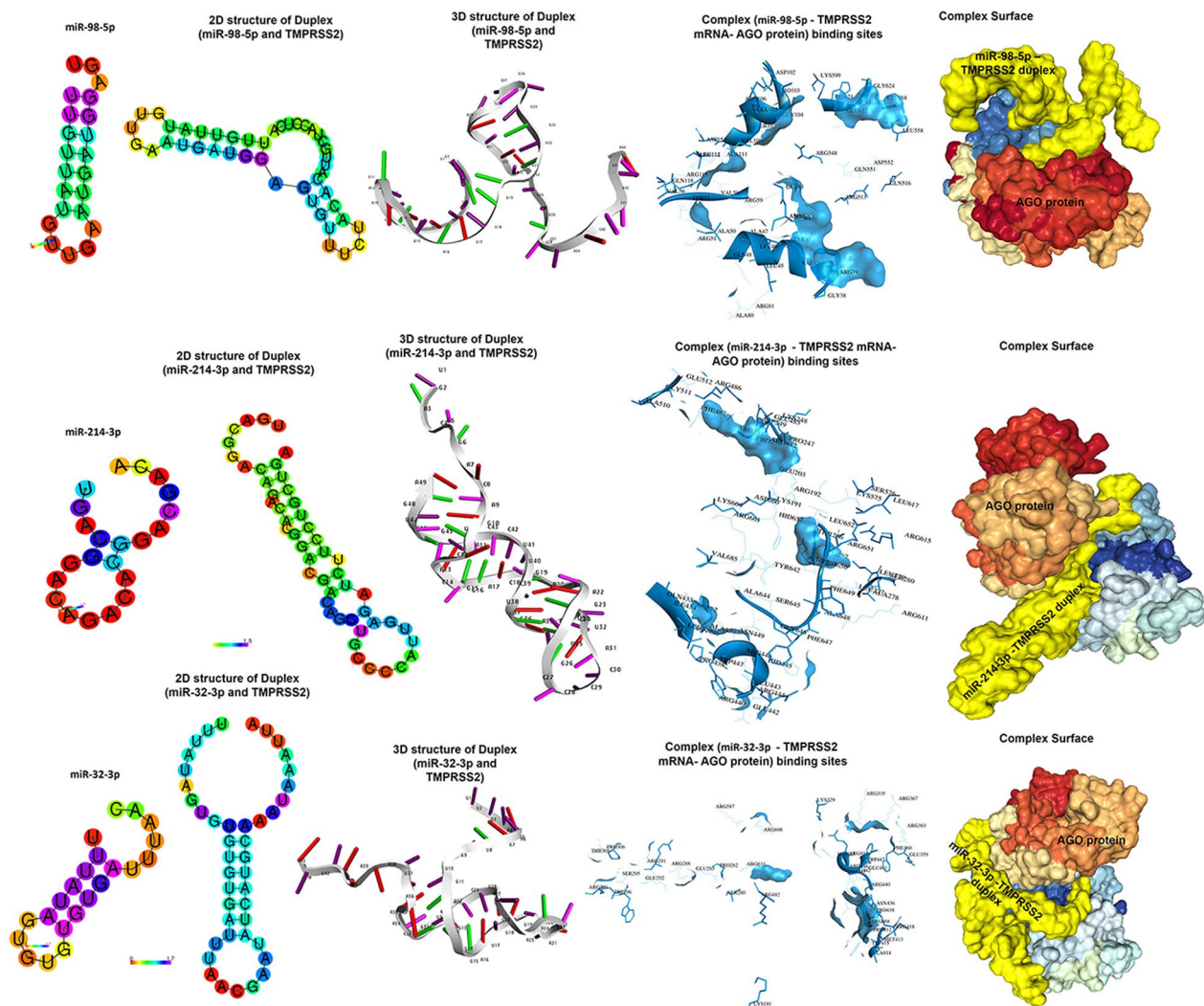


**Fig. 4** 2D structural models of miR-98-5p, miR-214-3p and miR-32-3p; 2D and 3D structural models of different microRNAs (miR-98-5p, miR-214-3p and miR-32-3p) duplexes with mRNA of TMPRSS2 gene; Binding sites interactions between amino acid residues of Argonaut protein and microRNAs- TMPRSS2 duplexes and surface shape of argonaut silencing complexes

reduced the overall intensity of the immunoreaction to an overall mild reaction across the alveolar cells, revealing a significant difference in expression ( $p < 0.05$  versus the control group and  $p < 0.001$  versus the COVID-19 group) (Fig. 11c). Similar to TMPRSS2, we observed mild immunoreactivity for ACE2 in the alveolar cells of the control group (Fig. 11e). In contrast, intense immunoreactivity was noted in the COVID-19 group (Fig. 11f). In the MSC-EV-treated group, a mild reaction was observed in the alveolar cells (Fig. 11g). These results were confirmed by imaging analysis of the intensity of TMPRSS2 and ACE2 immunoreactivity (Fig. 11d, h). Immunoreactivity in the COVID-19 group was  $p < 0.001$  versus that in the control group, whereas

immunoreactivity in the MSC-EV-treated group was  $p < 0.001$  versus the COVID-19 group.

#### SARS-CoV-2 protein expression in SARS-CoV-2-infected lungs decreased following MSC-EV administration

Immunohistochemical staining for the SARS-CoV-2 virus revealed negative immune reactivity in the control lungs (Fig. 12a). Lung sections from the COVID-19 group revealed intense brown granular cytoplasmic reactions in the alveolar cells (Fig. 12b). The lung sections from the MSC-EV-treated group displayed milder, less intense, cytoplasmic reactions across fewer alveoli cells (Fig. 12c). Histological observations were confirmed by image analysis of the intensity of SARS-CoV-2 immunoreactivity

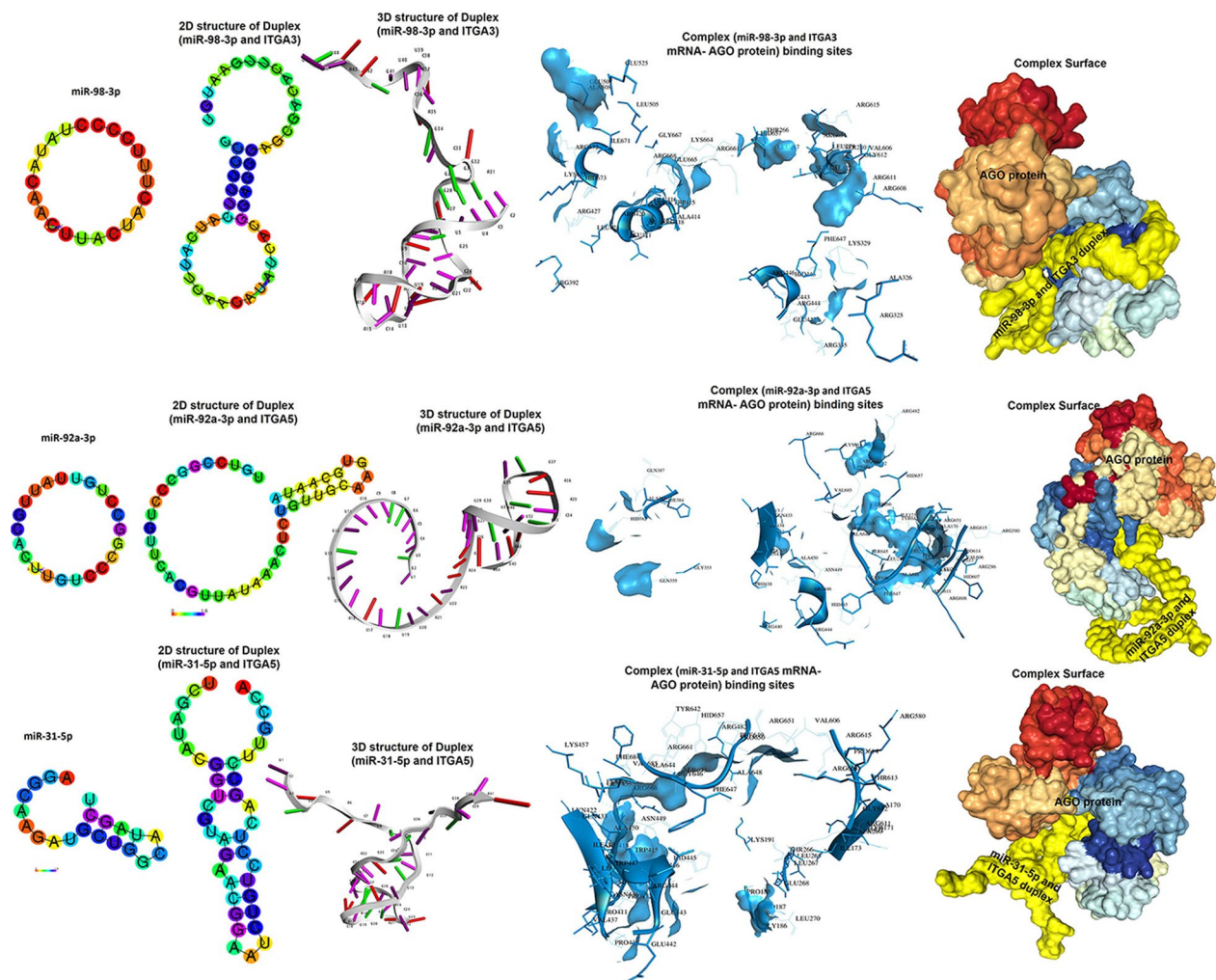


**Fig. 5** 2D structural models of miR-98-3p, miR-92a-3p and miR-31-5p; 2D and 3D structural models of miR-98-3p with mRNA of ITGA3 gene and miR-92a-3p, miR-31-5p with mRNA of ITGA5 gene; Binding sites interactions between amino acid residues of Argonaute protein and microRNAs- ITGA duplexes and surface shape of argonaute silencing complexes

(Fig. 12d). All scores for SARS-CoV-2 immune expression were  $p < 0.001$  versus the control group for the COVID-19 group and  $p < 0.001$  versus the COVID-19 group for the MSC-EV-treated group.

#### MSCs-EVs alleviated histopathological aberrations in SARS-CoV-2-infected lung tissue

Examination of H&E-stained lung sections from the control group (group I) revealed a normal alveolar structure with patent lumens and thin interalveolar septa, lined predominantly by squamous type I pneumocytes and a few large cuboidal type II pneumocytes. Alveolar capillaries were also observed (Fig. 13a). The COVID-19 group (group II) displayed marked histological alterations. Diffuse consolidation of the lung tissue with marked thickening of the interalveolar septa, abundant inflammatory cells and collapsed lumens, in addition to intra-alveolar

hemorrhage and congested blood vessels, were observed (Fig. 13b). Treatment of the infected hamsters in group III with MSCs-EVs resulted in a marked amelioration of the alterations. Most alveolar lumens appeared patent with a reduction in the interalveolar septa thickness and inflammatory cells, except for a few residual areas with congested blood vessels (Fig. 13c). Statistical analysis of the lung injury observed in the H&E-stained COVID-19 lung sections revealed a statistically significant increase in all measured parameters compared with those in the control group ( $p < 0.001$ ). In contrast, these parameters were significantly reduced following MSC-EV administration (Fig. 13d) ( $p < 0.001$ ). Masson's trichrome-stained lung sections from the control group (group I) revealed the presence of fine collagen fibers in the interalveolar septa and surrounding the bronchioles and blood vessels (Fig. 13e). Conversely, in the SARS-CoV-2-infected lungs,



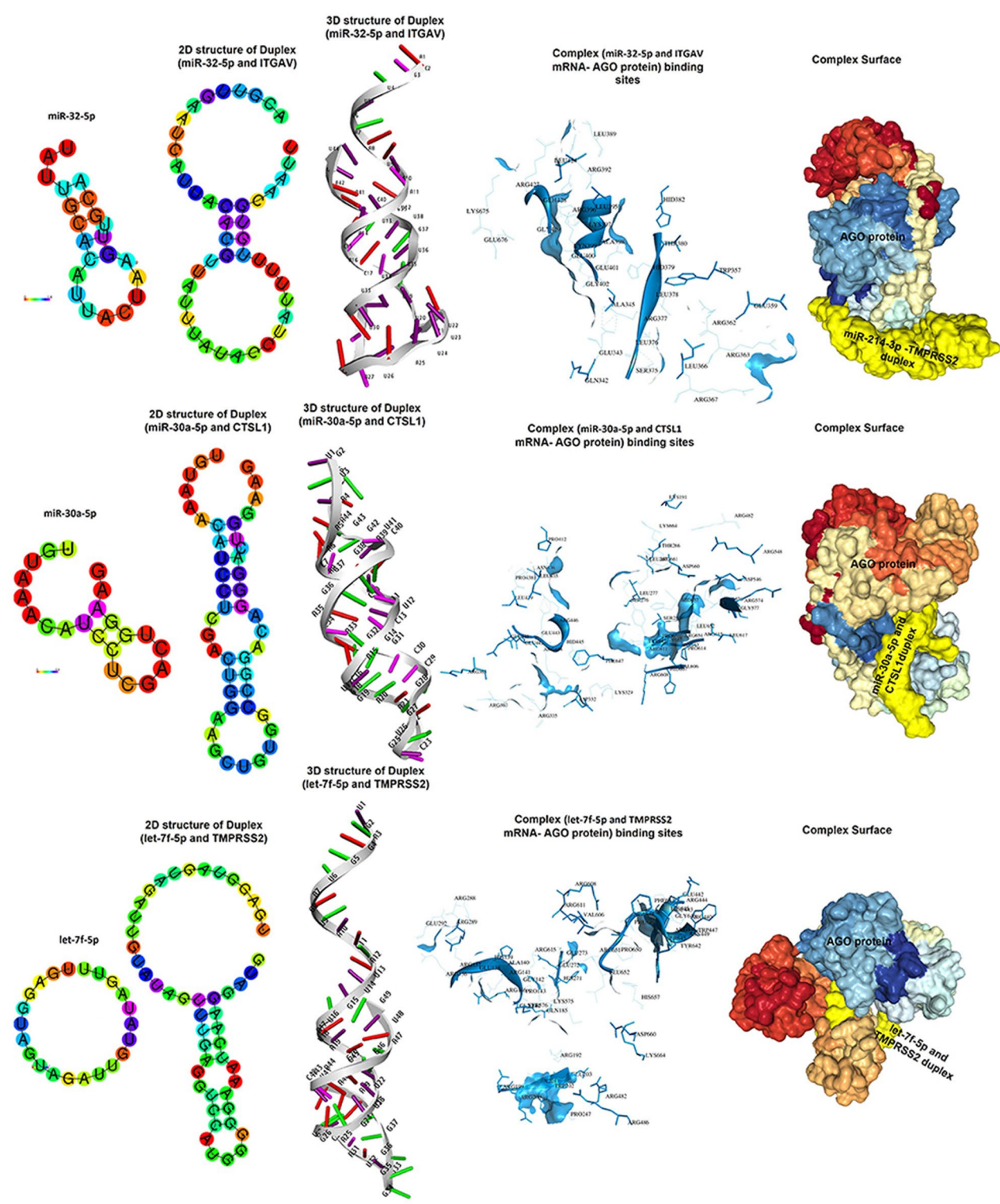


**Fig. 6** 2D structural models of miR-32-5p, miR-30a-5p and let-7f-5p; 2D and 3D structural models of miR-32-5p with mRNA of ITGAV, miR-30a-5p with mRNA of CTSL1, let-7f-5p with mRNA of TMPRSS2 gene; Binding sites interactions between amino acid residues of Argonaute protein and microRNAs- ITGAV, CTSL1 and TMPRSS2 duplexes and surface shape of argonaute silencing complexes

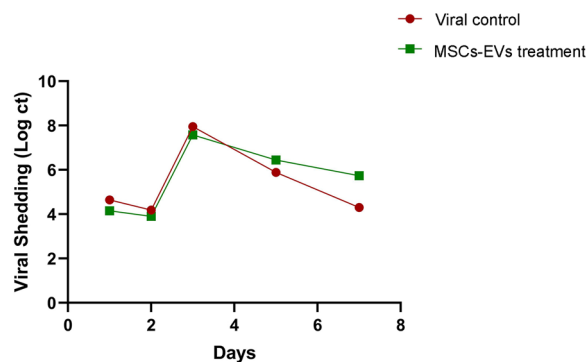


**Fig. 7** Viral shedding is unaltered following exosome treatment. Viral shedding from infected and infected + MSCs–EVs was determined at days 0, 2, 4, 6, and 8. The x-axis indicates time (days), and y-axis indicates Viral Shedding (log ct)

abundant intensely stained collagen fibers were observed in the thickened interalveolar septa and surrounding the bronchioles (Fig. 13f). In the lungs of the MSC–EV-treated hamsters, fine intensely stained collagen fibers were observed in the interalveolar septa and around the blood vessels (Fig. 13g). Compared with the control treatment, the administration of MSCs–EVs led to a significant reduction ( $p < 0.05$ ) in the surface area of collagen deposition (Fig. 13h) ( $p < 0.001$ ).

## Discussion

The treatment of COVID-19 remains a challenge, and effective therapies for the rapidly mutating SARS-CoV-2 virus are urgently needed. One potential approach is the

use of cell-based therapies, particularly MSC-derived extracellular vehicles (EVs), as a cell-free alternative to MSC therapy. Recent clinical research has demonstrated that MSC-derived EVs can decrease the production of proinflammatory cytokines and support the restoration of lung integrity, indicating that the MSC-secretome, which includes EVs, is a high-quality, safe, and potent therapeutic agent for COVID-19 treatment [42].

In our study, the injection of MSCs–EVs alleviated the histopathological changes in hamsters infected with SARS-CoV-2 by reducing the inflammatory response, decreasing interalveolar septa thickening, preventing lumen collapse, reducing intra-alveolar hemorrhage, and decongesting blood vessels. These observations were reinforced by the fact that the MSC–EV group displayed reduced systemic inflammation, as indicated by a decrease in CRP levels, a reduced neutrophil/leukocyte ratio, and a reduced total white blood cell count. Taken together, these results revealed that systemic inflammation and histological abnormalities were significantly reduced in the MSC–EV-treated SARS-CoV-2-infected animals.

The roles of MSC–EV-derived microRNAs (miRNAs) are partially understood, but their functions in the context of host–virus interactions during viral infections are likely more complex. miRNAs play crucial roles as regulators of viral pathogenesis by affecting host–virus interactions and modulating host miRNA expression [43, 44]. This interaction between the virus and host miRNAs can alter the transcriptome of host cells and indirectly impact viral infections by influencing cellular pathways that have

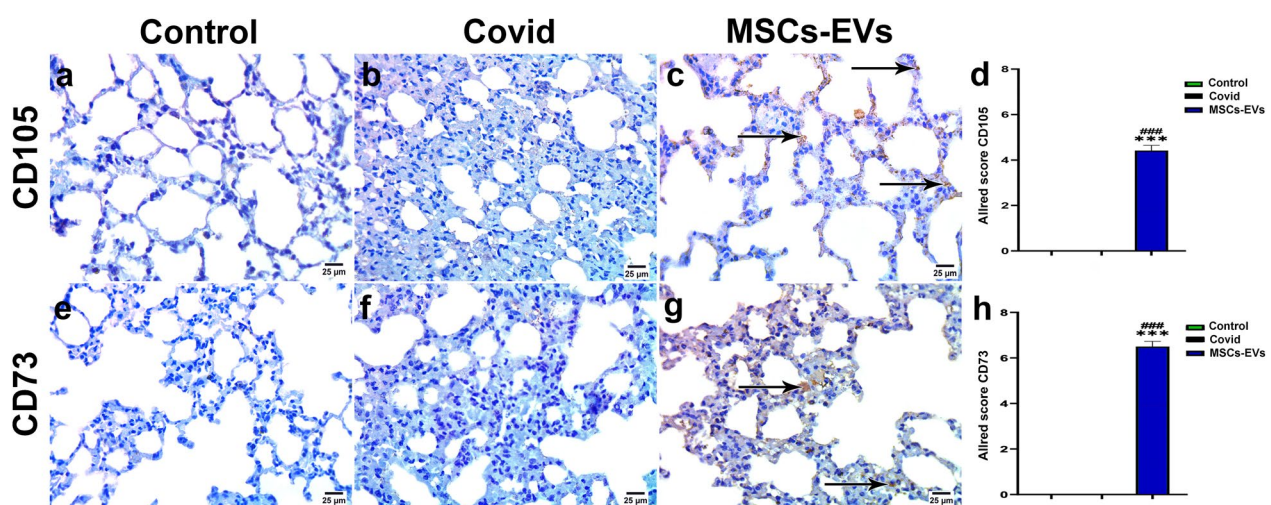


**Fig. 8** Immunohistochemical reaction for MSCs–EVs localization in lung tissues. **a** control group: negative immune reaction for CD105, **b** covid group: negative immune reaction for CD105, **c** MSCs–EVs group: Strong immune reaction for CD105 (arrow). **d** Allred score for CD105 expressed as mean ± SEM. \*\*\* $p < 0.001$  versus the control group, ### $p < 0.001$  versus the covid group. **e** control group: negative immune reaction for CD73, **f** covid group: negative immune reaction for CD73, **g** MSCs–EVs group: Strong immune reaction for CD73 (arrow). **h** Allred score for CD73 expressed as mean ± SEM. \*\*\* $p < 0.001$  versus the control group, ### $p < 0.001$  versus the covid group

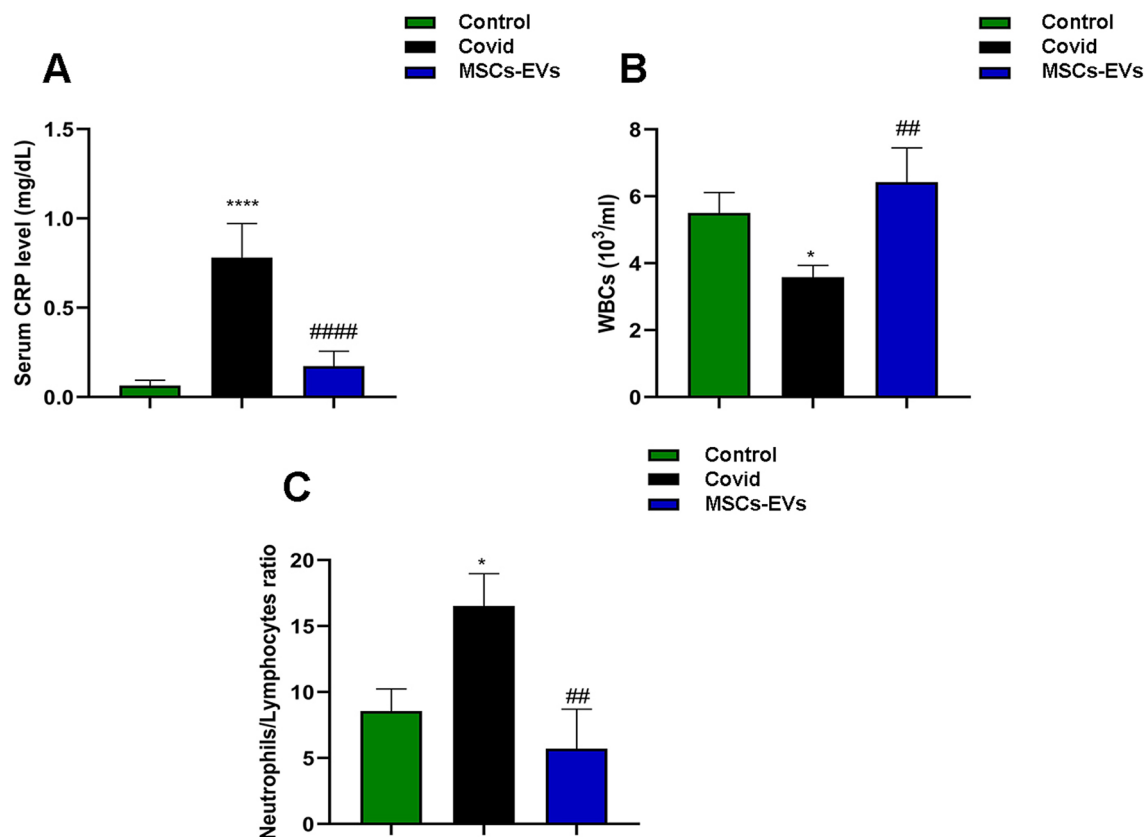


**Fig. 9** MSC-EVs administration reduces covid induced inflammatory responses. **a** Serum CRP; **b** serum WBCs; **c** Serum neutrophil /lymphocyte. Data are expressed as mean  $\pm$  SEM. \* $p < 0.05$  versus the control group, \*\*\*\* $p < 0.0001$  versus the control group, ## $p < 0.01$  versus the covid group, #### $p < 0.0001$  versus the covid group

broad pro- or antiviral effects [45]. In the case of SARS-CoV-2, several miRNAs that can regulate the expression of proteins involved in viral entry pathways, such as ACE2, TMPRSS2, RAB14, integrin, and cathepsin L, have been identified [46]. Therefore, targeting these host miRNAs involved in viral entry and replication could provide a viable approach for developing new treatments against SARS-CoV-2 [47–51].

Several strategies have been developed to disrupt the interaction between ACE2 receptors and SARS-CoV-2, with the aim of blocking the spread of infection [52]. In the present study, there was a significant increase in ACE2 immunoexpression in the lung tissues of SARS-CoV-2-infected hamsters. However, compared with infected hamsters, hamsters treated with MSC-EVs presented significant decreases in ACE2 immuno-expression. We propose that MSC-EV-derived miR-200c could be used as a preventive medication by reducing ACE2 expression. We observed an increase in the expression of miR-200c-3p, as well as other MSC-EV miRNAs, including miR-26b-5p, miR-125b-5p, miR-17-5p, miR-27b-3p, and miR-143-3p, in the groups treated with

MSC-EVs. The relationship between ACE2 and miR-200c has been investigated, and in cardiomyocytes, Ace2 directly targets miR-200c [48, 49, 51]. Previous studies have shown that hsa-miR-17 targets viral proteins, including the S, N, Orf1a, M, and E proteins, and that its expression is suppressed during viral replication [48, 50]. Recent reports have shown that the level of miR-17-5p is reduced, whereas the level of miR-27a-3p is increased in the plasma of COVID-19 patients compared with healthy blood donors [53]. Furthermore, Demiray et al. [54] reported lower expression levels of hsa-miR-17 and hsa-miR-200c in COVID-19 patients than in healthy individuals. Furthermore, Chen et al. [55] demonstrated that miR-27b directly targets specific binding sites in the 3'-UTR of ACE transcripts to decrease ACE expression. Wicik et al. [56] identified miR-27a-3p as one of the major miRNAs modulating ACE2 networks. Additionally, Pierce et al. [57] reported that hsa-miR-27a-3p influences the ACE2 network, thereby influencing the course of infection. These findings support the findings of the present study of the downregulation of miR-27 in infected hamsters and the significant increase in miR-27



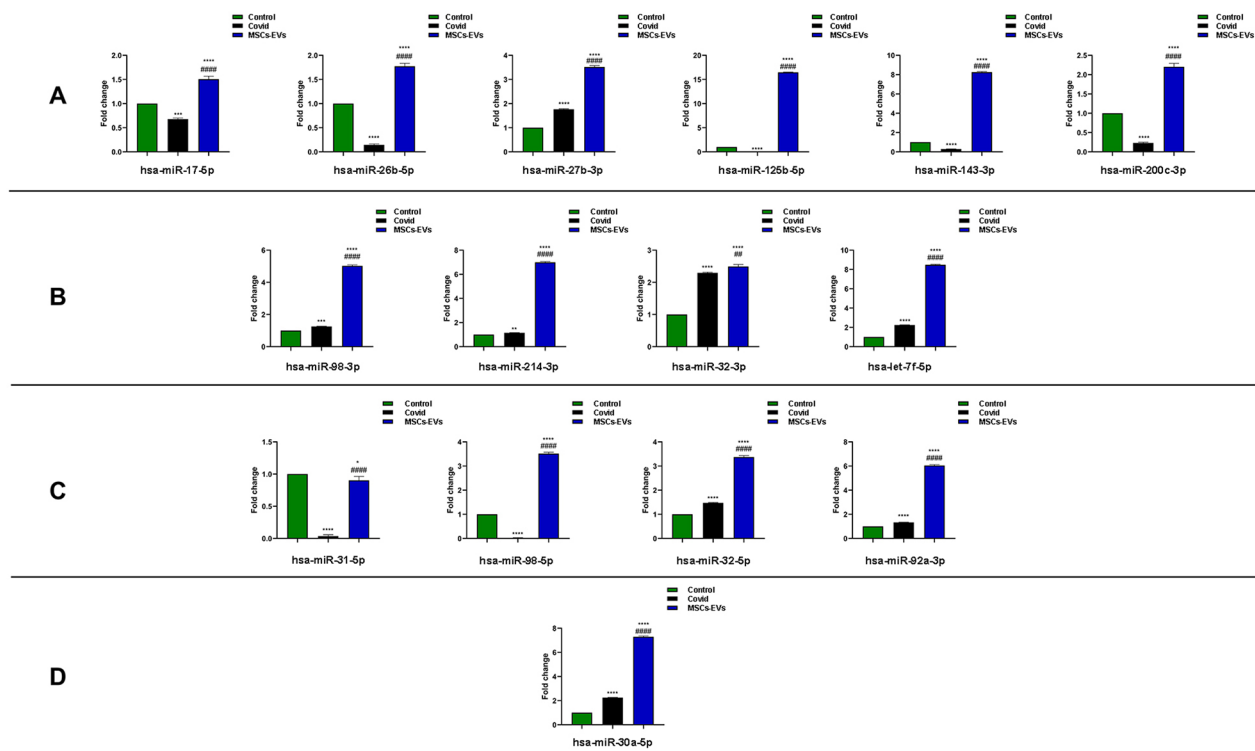


**Fig. 10** MSC-EVs and their role in miRNA expression regulation. **a** Fold change of ACE2 receptor interacting microRNAs miR-17-5p, miR-26b-5p, miR-27b-3p, miR-125b-5p, miR-143-3p and miR-200c-3p in control, covid and MSC-EVs groups.; **b** Fold change of TMPRSS2 receptor interacting microRNAs miR-98-5p, miR-214-3p, miR-32-3p and let-7f-5p in control, covid and MSC-EVs groups. **c** Fold change of ITGA receptors interacting microRNAs miR-31-5p, miR-98-5p, miR-32-5p and miR-92a-3p in control, covid-infected and MSC-EVs groups.; **d** Fold change of CTSL1 receptor interacting microRNA miR-30a-5p in control, covid and MSC-EVs groups. Data are expressed as mean  $\pm$  SEM. \* $p < 0.05$  versus the control group, \*\* $p < 0.01$  versus the control group, \*\*\* $p < 0.001$  versus the control group, \*\*\*\* $p < 0.0001$  versus the control group, # $p < 0.05$  versus the covid group, ## $p < 0.01$  versus the covid group, ### $p < 0.001$  versus the covid group, #### $p < 0.0001$  versus the covid group

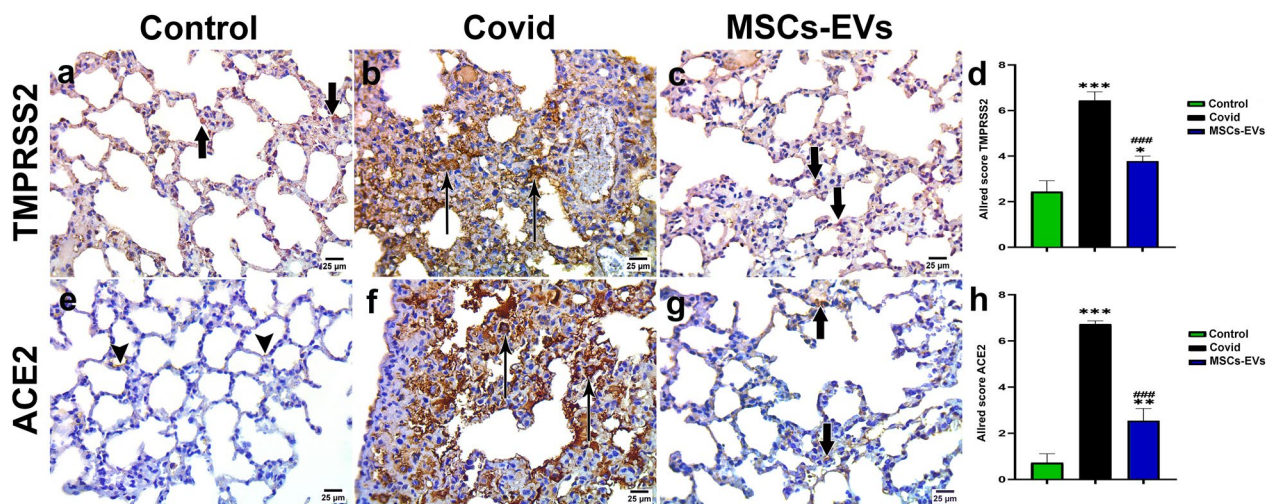


**Fig. 11** Representative photomicrographs of lung immune stained sections for **a-c** TMPRSS2 expression **a** Control group: moderate immune expression (bold arrow) **b** Covid group: intense brown granular cytoplasmic positivity (arrow) in the alveolar cells **c** MSCs-EVs group: mild to moderate brown granular cytoplasmic positivity (bold arrow) in the alveolar cells. **e-f** ACE2 expression **e** Control group: mild immunoreactivity in some alveolar cells. **f** Covid group: intense immunoreactivity in a large number of cells. **g** MSCs-EVs group: moderate reaction in the alveolar cells. **d** and **h** Allred score for TMPRSS2 and ACE2 expression. Data are expressed as mean  $\pm$  SEM. \* $p < 0.05$  versus the control group, \*\* $p < 0.01$  versus the control group, \*\*\* $p < 0.001$  versus the control group, ### $p < 0.001$  versus covid group. Allred index (0–1 = negative, 2–3 = mild, 4–6 = moderate, and 7–8 = strongly positive)



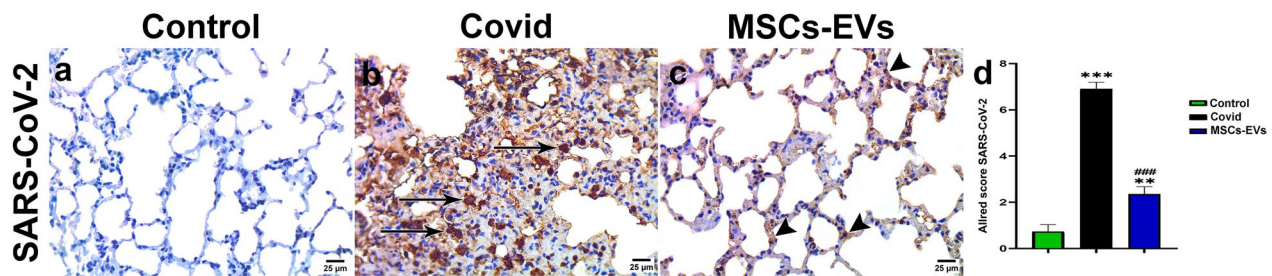


**Fig. 12** Representative photomicrographs from SARS-CoV-2 immune stained lung sections showing **a** Control group: negative immune reactivity **b** Covid group: intense brown granular cytoplasmic immune reactivity (arrow) in the alveolar epithelium **c** MSCs-EVs group: mild to moderate brown granular cytoplasmic positivity (arrowhead) in the alveolar epithelium. **d** Allred score for SARS-CoV-2 immune expression. Data are expressed as mean ± SEM. \*\*\* $p < 0.001$  versus the control group, \*\*\* $p < 0.001$  versus the covid group, #### $p < 0.0001$  versus the covid group. Allred index (0–1 = negative, 2–3 = mild, 4–6 = moderate, and 7–8 = strongly positive)

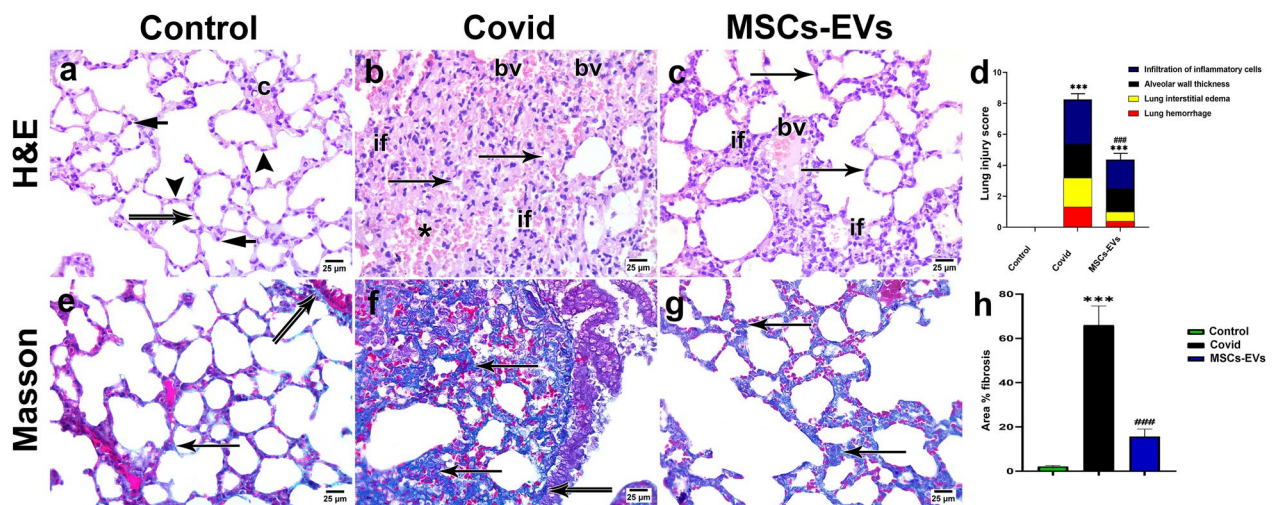


**Fig. 13** Representative photomicrographs from (a–c) hematoxylin and eosin and (e–g) Masson trichrome stained lung sections. H&E: **a** Control group: patent alveolar lumens and thin interalveolar septa (double arrow) lined by squamous type I pneumocytes (arrowhead) and large cuboidal type II pneumocytes (short arrow). An alveolar capillary (c) is also seen. **b** Covid group: Lung consolidation with diffuse thickening of the interalveolar septa, abundant inflammatory cells (if), collapsed lumens (arrow), intra alveolar hemorrhage (asterisk) and congested blood vessels (bv). **c** MSCs-EVs group: with predominantly patent alveolar lumens and thin interalveolar septa (arrow) and residual thickening of the interalveolar septa with inflammatory cell infiltration (if) and congested blood vessels (bv). **d** Assessment of lung with the lung injury scoring system. Data are expressed as mean ± SEM. \*\*\* $p < 0.001$  versus the control group, #### $p < 0.0001$  versus the covid group. Masson trichrome: **e** Control group: fine collagen fibers in the interalveolar septa and surrounding the bronchioles and blood vessels. **f** Covid group: abundant, intensely staining collagen fibers in the thickened interalveolar septa (arrow) and surrounding the bronchioles (double arrow). **g** MSCs-EVs group: fine, intensely stained collagen fibers in the interalveolar septa (arrow) and around the blood vessels. **h** Mean area percentage of collagen fibers in the different experimental groups. Data are expressed as mean ± SEM. \*\*\* $p < 0.001$  versus the control group, #### $p < 0.0001$  versus the covid group

levels after MSC-EV administration, suggesting a role for miR-27 in regulating ACE2 receptors.

In recent research, miR-143 was found to be significantly associated with the human immune system and has potential as a therapeutic target for vaccination [58]. Studies have shown that miR-143 is expressed in smooth muscle cells and cardiomyocytes, indicating its role in these cell types as a negative regulator of ACE2, influencing the balance between the formation of Ang-(1–7) and Ang II degradation [59] Chen et al. [55]. Furthermore,

the upregulation of miR-143-3p expression reduces the levels of pulmonary inflammatory factors and decreases alveolar epithelial cell apoptosis in *Mycoplasma pneumoniae* via the inhibition of the TLR4/MyD88/NF-B signaling pathway [60]. miR-143 was closely associated with lung sepsis in both mouse and human leucocytes after the induction of LPS. Furthermore, Wang et al. [60] demonstrated that Ang II induces apoptosis and inflammation by regulating miR-143-3p in BEAS-2B cells, indicating that miR-143-3p suppresses ACE2 by targeting its

3'-UTR. These findings are consistent with those of the current study, where the modulation of ACE2 through miR-143-3p could be a novel approach for the management of lung inflammation.

Multiple studies have shown that miR-125b-5p inhibits the production of ACE2, reducing the ability of SARS-CoV-2 to enter cells. Wang et al. [60] confirmed this relationship by using TargetScan to predict that miR-125b targeted the 3'-UTR of ACE2 mRNA. They conducted luciferase reporter experiments, which demonstrated that miR-125b reduced the activity of the reporter carrying the wild-type ACE2 3'-UTR. These findings demonstrated that miR-125b directly targeted ACE2 and are concomitant with the results of the present study, with increased miR-125b-5p expression and significantly decreased ACE2 immuno-expression in the MSC-EV-treated group compared with those in the COVID-19 infected group.

Moreover, the TMPRSS2 receptor plays a crucial role in facilitating the invasion of the respiratory system by SARS-CoV-2, the virus responsible for COVID-19 [61] [62]. It is expressed in the epithelial cells of the human lung and is responsible for degrading the viral spike protein, particularly at the S1/S2 and S2' sites, which enables the fusion of host membranes [5, 63]. Studies using mouse models and human cell lines have shown that interventions aimed at reducing TMPRSS2 levels resulted in decreased viral invasion [64, 65]. Consequently, targeting TMPRSS2 suppression through miRNAs could be a valuable approach for managing COVID-19.

In their computational analysis, Khalaj et al. [66] identified microRNAs that specifically target TMPRSS2. Matarese et al. [61] confirmed that miR-98-5p effectively regulates TMPRSS2 transcription in different types of human endothelial cells, including those from the umbilical vein and the lung. Notably, miR-98 has been implicated in the pathogenesis of SARS-CoV, where it aids in viral transmission and replication by stimulating bronchoalveolar stem cell differentiation and downregulating ACE2 [48]. Previous reports have shown that miR-98 is affected by viral SARS-CoV nucleocapsid-driven downregulation, leading to impaired viral entry in alveolar cells [67]. Sardar et al. [68] reported that hsa-miR-98 targeted the spike protein in the SARS-CoV-2 genome. Additionally, Rota et al. [69] demonstrated the importance of miR-98-mediated targeting of the S protein in SARS-CoV-2.

TMPRSS2 is highly expressed in Caco-2 cells, facilitating the entry of SARS-CoV-2 [5]. miR-98 and miR-32 significantly reduce the levels of TMPRSS2 transcript and protein in Caco-2 cells, with miR-32 exhibiting the highest level of gene repression. These findings support the use of gene silencing strategies to investigate TMPRSS2-mediated viral entry in the host. Hoffmann suggested that

a TMPRSS2 inhibitor could be a potential therapeutic option for COVID-19. A number of studies have further demonstrated that miR-32-3p directly inhibits viral RNA at the protein level and exhibits secondary degradative activity in the influenza PB1 coding region [70]. In this context, miR-32-3p has promising therapeutic efficacy in targeting TMPRSS2 for the management of CoV-2 infections. Moreover, *in silico* research revealed that miR-32-5p and miR-92-3p are more complex posttranscriptional regulators than previously believed, as they are implicated in various biological processes crucial to the pathogenesis of SARS-CoV-2 [71]. For example, these microRNAs can target the lung cancer-related miRNA Rab-14 (RAB14), which has been identified as essential in lung cancer [72, 73]. RAB14, which is involved in the transport of membranes between endosomes and the Golgi complex, is closely linked to SARS-CoV-2 replication and plays a pivotal role in viral infection. Moreover, it may serve as a crucial protein for SARS-CoV-2 infection by assisting in the transport of vesicles necessary for the maturation and assembly of the virus's structural proteins [71]. The decreased levels of RAB14 transcripts and several other vital genes for SARS-CoV-2 infection observed in the lung biopsies of individuals with adenocarcinomas may be associated with increased levels of specific miRNAs [74].

These findings align with the outcomes of the present study, which revealed a significant increase in the levels of miR-32, miR-92, and miR-98, along with decreased levels of TMPRSS2 subsequent to MSC-MSC-EV administration. Consequently, the increased levels of miR-32-5p and miR-92-3 following MSC-MSC-EV treatment reduced TMPRSS2 but also suppressed the expression of Rab14 transcripts, suggesting a potential dual therapeutic strategy for COVID-19.

Let-7 family members play a role in the regulation of TMPRSS2; among these, let-7-5p is noteworthy. The increased expression of TMPRSS2 resulting from let-7 suppression suggested enhanced viral uptake into target cells through two mechanisms: first, the cleavage of SARS-S, which activates the S protein for membrane fusion, and second, the cleavage of ACE2 [75, 76]. Following virus internalization and replication, the membrane-bound ACE2 receptors degrade, leading to elevated levels of angiotensin II and the angiotensin type 1 receptor, which triggers an inflammatory immune response [77]. Reduced let-7 expression can contribute to the viral burden of the disease by facilitating viral entry into the host cell through increased TMPRSS2 expression and promoting inflammation via the NF-B/IL-6/let-7/LIN-28 axis. Furthermore, overexpression of let-7 mitigated the hyperinflammatory state. C163, as described by Xie et al. [78], is a small molecule that functions as a let-7 activator.

It can positively regulate let-7, thereby reducing viral proliferation and the release of proinflammatory cytokines. Promising results from in vitro experiments suggest the potential of this compound as a treatment for COVID-19 [78]. Consistent with these findings, our research revealed that the administration of MSC-EVs led to an increase in let-7-5p transcript levels, indicating that these EVs serve as let-7 stimulators against COVID-19.

The spike protein of SARS-CoV-2 contains a novel K403R substitution that introduces an RGD motif, which interacts with integrins  $\alpha_5\beta_1$  and  $\alpha V\beta_3$  [79]. These integrins, which are found on vascular endothelial cells, play a role in cell adhesion and the immune response [80]. Inhibiting the binding of SARS-CoV-2 to these integrins via peptides such as ATN-161 and cilengitide reduces viral infectivity and attenuates vascular inflammation [81–83]. miR-31 regulates integrin expression and function by targeting  $\beta_1$  and  $\beta_3$  integrins [84]. Direct binding of the spike protein to integrins activates inflammatory responses and increases leukocyte adhesion to the endothelium [83]. Blocking the integrin receptors  $\alpha_5\beta_1$  and  $\alpha V\beta_3$  restores barrier function and reduces inflammation [82, 83]. These findings suggest that integrins  $\alpha_5\beta_1$  and  $\alpha V\beta_3$  could be potential targets to prevent SARS-CoV-2 infection [81–83]. The interaction between integrin  $\alpha_5\beta_1$  and ACE2 may amplify cell adhesion signaling and increase viral infectivity [81]. Additionally, ACE2 and integrin  $\beta_1$  are upregulated in patients with COVID-19 and other relevant health conditions [79, 83]. These results are consistent with the results of the present study, as miR-31 is an MSC–MSC–EV microRNA that is expressed at high transcript levels in lung tissues after MSC–EVs administration [84]. Hence, the ameliorative effect of MSC–EVs could be attributed to the role of upregulated levels of miR-31 in suppressing integrin subunits [84].

Cathepsin L (CatL) is an enzyme found in lysosomes with various physiological roles, including apoptosis, antigen processing, and degradation of the extracellular matrix. It is also involved in the entry of SARS-CoV-2 into host cells. Inhibition of CatL is detrimental to SARS-CoV-2 infection and may affect later stages of infection [85]. Studies have demonstrated that CatL plays a significant role in the initial inflammatory response by activating M1 macrophages [86, 87]. This activation may contribute to the onset of the cytokine storm observed in conditions such as sepsis-induced acute kidney damage [88]. Additionally, CatL has been identified as crucial for SARS-CoV-2 entry into host cells. The virus attaches to its receptor, causing conformational changes in the spike protein, which is then proteolytically processed by CatL in endosomes [89]. In previous investigations with caliciviruses, CatL inhibitors significantly reduced viral replication. Confocal microscopy studies have revealed that CatL inhibitors can trap viral capsid proteins

in endosomes during virus entry, suggesting that CatL and endosome maturation play crucial roles in calicivirus infection [90]. Currently, there are no specific medications available for treating SARS-CoV-2 infections. However, drugs that exhibit CatL inhibitory properties could offer potential therapeutic options for COVID-19 once it is established that CatL is indeed essential for viral entry and potentially late-stage infection [85]. A study by Zhao et al. [91] revealed a feedback loop between miRNA-200c and CatL (Cathepsin L). The overexpression of miRNA-200c reduced CatL expression, whereas the knockdown of miRNA-200c significantly increased CatL expression. CatL overexpression, in turn, downregulated miRNA-200c expression, but this effect was counteracted by miRNA-200c restoration. These findings suggest that miRNA-200c may play a role in regulating CatL levels [91]. This finding is consistent with the results of the present study, which revealed that the administration of MSC–EVs resulted in increased levels of miR-200 and decreased levels of CatL, with decreased immune expression levels of SARS-CoV-2.

While multiple microRNAs were involved in regulating the viral receptor, the in silico and in vivo evidence indicates that let-7-5p played the most critical role overall in the antiviral mechanism of MSCs–EVs by targeting the essential TMPRSS2 protease for SARS-CoV-2 entry into host cells. Reduced levels of let-7-5p increase TMPRSS2 expression, enhancing viral uptake by activating the spike (S) protein and facilitating viral entry via cleavage of the ACE2 receptor. Overexpression of let-7-5p reduces TMPRSS2 expression, limiting viral entry and proliferation, and mitigating hyperinflammation, offering promising strategies for COVID-19 treatment.

## Conclusions

The current study revealed that MSCs–EVs effectively inhibited SARS-CoV-2 infection. The combination of the microRNA expression data, the protein expression results, and the viral load observations, aligned with in silico data, provided a robust and direct demonstration of the mechanism by which MSC–EVs can suppress SARS-CoV-2 entry and infection in the lung tissue. Our computational analysis indicated that the specific miRNAs contained in these targeted MSC–EVs strongly bind to relevant receptors, suggesting their potential as therapeutic targets for SARS-CoV-2 infection. Furthermore, the in vivo findings demonstrated that MSCs–EVs have the ability to prevent SARS-CoV-2 from entering host cells by modulating the expression of miRNAs, ACE2 and TMPRSS2 receptors, as well as modulating viral protein expression.

## Acknowledgements

The authors acknowledge technical and financial support from the Ministry of Education and the University of Hafr Al Batin, Saudi Arabia. The authors also thank AlMaarefa University, Riyadh, Saudi Arabia, for supporting this research.

### Author contributions

NE and OAB designed and planned the study. NE, NRF, RFS, OAB, DS, IE, AAD & FEA performed the experiments. NE, IE, OAB, FEA and HAA collected the data, and OAB, AAD, IE, DS, FEA, MES, NRF and HAA analyzed the data., NE, OAB, AAD, NRF & FEA wrote the manuscript. All authors read and approved the final manuscript.

### Funding

This research was funded by an institutional fund project (0061–1443-S). Therefore, the authors gratefully acknowledge technical and financial support from the ministry of education and the University of Hafr Al Batin, Saudi Arabia.

### Availability of data and materials

The data supporting this study's findings are available from the authors upon reasonable request from the corresponding author.

### Declarations

#### Ethics approval and consent to participate

This study was carried out in strict accordance with the recommendations in the Guide for the Care and Use of Laboratory Animals of the National Institutes of Health (NIH publication No. 85–23, revised 1996). The institutional animals' care approved all protocols and used the committee and research ethics board of the Faculty of Veterinary, Benha University, Egypt. The project title is IACUCREB, the approval number is BUFVTM, and the approval date is 13/4/2022.

#### Consent for publication

Not applicable.

#### Competing interests

Authors declare that they have no known competing financial interests or personal relationships that could have appeared to influence the work reported in this paper.

#### Author details

<sup>1</sup>Department of Clinical Laboratory Sciences, College of Applied Medical Sciences, University of Hafr Albatin, Hafr Al-Batin, Saudi Arabia. <sup>2</sup>Department of Medical Histology and Cell Biology, Faculty of Medicine, Zagazig University, Zagazig, Egypt. <sup>3</sup>Department of Medical Biochemistry and Molecular Biology, Faculty of Medicine, Benha University, Benha, Egypt. <sup>4</sup>Researcher of Pathology, Animal Health Research Institute, Agriculture Research Center, Giza, Egypt. <sup>5</sup>Department of Basic Medical Sciences, College of Medicine, AlMaarefa University, P.O. Box 71666, 11597 Riyadh, Saudi Arabia. <sup>6</sup>Department of Anatomy, Faculty of Medicine, Mansoura University, Mansoura, Egypt. <sup>7</sup>Department of Pharmacology and Toxicology, Faculty of Pharmacy, Al-Azhar University, Assiut Branch, Assiut, Egypt. <sup>8</sup>Department of Genetics and Genetic Engineering, Faculty of Agriculture, Benha University, Benha, Egypt. <sup>9</sup>Department of Medical Biochemistry and Molecular Biology, Faculty of Medicine, Mansoura University, Mansoura, Egypt. <sup>10</sup>PhD Molecular Genetics, Vice Principals' Office, Kings College, University of Aberdeen, Aberdeen AB24 3FX, UK. <sup>11</sup>Department of Medical Histology and Cell Biology Faculty of Medicine, Benha University, Benha, Egypt. <sup>12</sup>Stem Cell Unit, Faculty of Medicine, Benha University, Benha, Egypt. <sup>13</sup>Faculty of Medicine, Benha National University, Al Obour City, Egypt. <sup>14</sup>Cell and Tissue Engineering, School of pharmacy and bioengineering, Keele University, Keele, UK.

Received: 25 March 2024 Accepted: 20 August 2024

Published online: 20 September 2024

### References

- Casella M, Rajnik M, Aleem A, Dulebohn SC, Di Napoli R. Features, evaluation, and treatment of coronavirus (COVID-19). *StatPearls* [internet]. StatPearls publishing; 2023.
- Cucinotta D, Vanelli M. WHO declares COVID-19 a pandemic. *Acta Bio med Atenei Parm Mattioli*. 1885;2020(91):157.
- Mohammed MA. Fighting cytokine storm and immunomodulatory deficiency: by using natural products therapy up to now. *Front Pharmacol*. 2023;14:1111329.
- Ali FEM, Mohammedsaleh ZM, Ali MM, Ghogor OM. Impact of cytokine storm and systemic inflammation on liver impairment patients infected by SARS-CoV-2: prospective therapeutic challenges. *World J Gastroenterol*. 2021;27:1531.
- Hoffmann M, Kleine-Weber H, Schroeder S, Krüger N, Herrler T, Erichsen S, et al. SARS-CoV-2 cell entry depends on ACE2 and TMPRSS2 and is blocked by a clinically proven protease inhibitor. *Cell*. 2020;181:271–80.
- Padmanabhan P, Desikan R, Dixit NM. Targeting TMPRSS2 and Cathepsin B/L together may be synergistic against SARS-CoV-2 infection. *PLoS Comput Biol*. 2020;16:e1008461.
- Li G, Hilgenfeld R, Whitley R, De Clercq E. Therapeutic strategies for COVID-19: progress and lessons learned. *Nat Rev Drug Discov*. 2023;22:449–75.
- Raman R, Patel KJ, Ranjan K. COVID-19: unmasking emerging SARS-CoV-2 variants, vaccines and therapeutic strategies. *Biomolecules*. 2021;11:993.
- Askenase PW. COVID-19 therapy with mesenchymal stromal cells (MSC) and convalescent plasma must consider exosome involvement: Do the exosomes in convalescent plasma antagonize the weak immune antibodies? *J Extracell Vesicles*. 2020;10:e12004.
- Pocsfalvi G, Mammadova R, Ramos Juarez AP, Bokka R, Trepiccione F, Capasso G. COVID-19 and extracellular vesicles: an intriguing interplay. *Kidney Blood Press Res*. 2020;45:661–70.
- Schultz IC, Bertoni APS, Wink MR. Mesenchymal stem cell-derived extracellular vesicles carrying miRNA as a potential multi target therapy to COVID-19: an in silico analysis. *Stem Cell Rev Rep*. 2021;17:341–56.
- Panda M, Kalita E, Singh S, Kumar K, Rao A, Prajapati VK. MiRNA-SARS-CoV-2 dialogue and prospective anti-COVID-19 therapies. *Life Sci*. 2022;305:120761.
- Maranini B, Ciancio G, Ferracin M, Cultrera R, Negrini M, Sabbioni S, et al. microRNAs and inflammatory immune response in SARS-CoV-2 infection: a narrative review. *Life*. 2022;12:288.
- Kalayinia S, Arjmand F, Maleki M, Malakootian M, Singh CP. MicroRNAs: roles in cardiovascular development and disease. *Cardiovasc Pathol*. 2021;50:107296.
- Lu TX, Rothenberg ME. MicroRNA. *J Allergy Clin Immunol*. 2018;141:1202–7.
- Pozniak T, Shcharbin D, Bryszewska M. Circulating microRNAs in medicine. *Int J Mol Sci*. 2022;23:3996.
- Ho PTB, Clark IM, Le LTT. MicroRNA-based diagnosis and therapy. *Int J Mol Sci*. 2022;23:7167.
- Saliminejad K, Khorram Khorshid HR, Soleymani Fard S, Ghaffari SH. An overview of microRNAs: biology, functions, therapeutics, and analysis methods. *J Cell Physiol*. 2019;234:5451–65.
- Selbach M, Schwanhäusser B, Thierfelder N, Fang Z, Khanin R, Rajewsky N. Widespread changes in protein synthesis induced by microRNAs. *Nature*. 2008;455:58–63.
- Ahmad W, Gull B, Baby J, Panicker NG, Khader TA, Akhlaq S, et al. Differentially-regulated miRNAs in COVID-19: a systematic review. *Rev Med Virol*. 2023;33:e2449.
- Fadaka AO, Pretorius A, Klein A. MicroRNA assisted gene regulation in colorectal cancer. *Int J Mol Sci*. 2019;20:4899.
- Agrawal P, Singh H, Srivastava HK, Singh S, Kishore G, Raghava GPS. Benchmarking of different molecular docking methods for protein-peptide docking. *BMC Bioinform*. 2019;19:105–24.
- Schneidman-Duhovny D, Inbar Y, Nussinov R, Wolfson HJ. PatchDock and SymmDock: servers for rigid and symmetric docking. *Nucleic Acids Res*. 2005;33:W363–7.
- Gomaa MR, El Rifay AS, Shehata M, Kandeil A, Nabil Kamel M, Marouf MA, et al. Incidence, household transmission, and neutralizing antibody seroprevalence of Coronavirus Disease 2019 in Egypt: results of a community-based cohort. *PLoS Pathog*. 2021;17:e1009413.
- Bahr MM, Amer MS, Abo-EL-Sooud K, Kamel SM, Fouly MA, Abdallah AN. Effect of topical application of lyophilized xenogenous mesenchymal stem cell-derived extracellular vesicles on central and peripheral corneal ulcers healing in rabbits. *Adv Anim Vet Sci*. 2023;11:132–40.
- Rafat A, Gadallah SM, Misk TN, Fadel MS, Abdallah AN, Sharshar A. Potential regenerative effect of mesenchymal stem cells-derived microvesicles



- on healing of the ruptured achilles tendon in a dog model. *J Curr Vet Res*. 2022;4:140–51.
27. Imai M, Iwatsuki-Horimoto K, Hatta M, Loeber S, Halfmann PJ, Nakajima N, et al. Syrian hamsters as a small animal model for SARS-CoV-2 infection and countermeasure development. *Proc Natl Acad Sci*. 2020;117:16587–95.
  28. Blaurock C, Breithaupt A, Weber S, Wylezich C, Keller M, Mohl B-P, et al. Compellingly high SARS-CoV-2 susceptibility of Golden Syrian hamsters suggests multiple zoonotic infections of pet hamsters during the COVID-19 pandemic. *Sci Rep*. 2022;12:15069.
  29. Kutkat O, Moatasim Y, Al-Karmalawy AA, Abulkhair HS, Gomaa MR, El-Taweel AN, et al. Robust antiviral activity of commonly prescribed antidepressants against emerging coronaviruses: in vitro and in silico drug repurposing studies. *Sci Rep*. 2022;12:12920.
  30. Bruno S, Grange C, Collino F, Deregibus MC, Cantaluppi V, Biancone L, et al. Microvesicles derived from mesenchymal stem cells enhance survival in a lethal model of acute kidney injury. *PLoS ONE*. 2012;7:e33115.
  31. Perera RA, Wang P, Gomaa MR, El-Shesheny R, Kandeil A, Bagato O, et al. Seroprevalence for MERS coronavirus using microneutralisation and pseudoparticle virus neutralisation assays reveal a high prevalence of antibody in dromedary camels in Egypt, June 2013. *Eurosurveillance*. 2013;18:20574.
  32. Teilmann AC, Nygaard Madsen A, Holst B, Hau J, Rozell B, Abelson KSP. Physiological and pathological impact of blood sampling by retro-bulbar sinus puncture and facial vein phlebotomy in laboratory mice. *PLoS ONE*. 2014;9:e113225.
  33. Ebrahim N, Al Saihati HA, Mostafa O, Hassouna A, Abdulsamea S, Abd El Aziz M, El Gebaly E, et al. Prophylactic evidence of MSCs-derived exosomes in doxorubicin/trastuzumab-induced cardiotoxicity: beyond mechanistic target of NRG-1/Erb signaling pathway. *Int J Mol Sci*. 2022;23:5967.
  34. Ebrahim N, Al Saihati HA, Shaman A, Dessouky AA, Farid AS, Hussien NI, et al. Bone marrow-derived mesenchymal stem cells combined with gonadotropin therapy restore postnatal oogenesis of chemo-ablated ovaries in rats via enhancing very small embryonic-like stem cells. *Stem Cell Res Ther*. 2021;12:1–19.
  35. Suvarna KS, Layton C, Bancroft JD. Bancroft's theory and practice of histological techniques E-Book. Elsevier Health Sciences; 2018.
  36. S Kim S. Bancroft's theory and practice of histological techniques eighth edition/S. Kim Suvarna. Elsevier Limited; 2019.
  37. Schindelin J, Arganda-Carreras I, Frise E, Kaynig V, Longair M, Pietzsch T, et al. Fiji: an open-source platform for biological-image analysis. *Nat Methods*. 2012;9:676–82.
  38. Huang R, Shi Q, Zhang S, Lin H, Han C, Qian X, et al. Inhibition of the cGAS-STING pathway attenuates lung ischemia/reperfusion injury via regulating endoplasmic reticulum stress in alveolar epithelial type II cells of rats. *J Inflamm Res*. 2022;15:5103–19. <https://doi.org/10.2147/JIR.S365970>.
  39. Schindelin J, Rueden CT, Hiner MC, Eliceiri KW. The ImageJ ecosystem: an open platform for biomedical image analysis. *Mol Reprod Dev*. 2015;82:518–29. <https://doi.org/10.1002/mrd.22489>.
  40. Bankhead P, Loughrey MB, Fernández JA, Dombrowski Y, McArt DG, Dunne PD, et al. QuPath: open source software for digital pathology image analysis. *Sci Rep*. 2017;7:1–7.
  41. Dorus B. Development of a freeze-drying strategy to store human bone marrow mesenchymal stem/stromal derived extracellular vesicles for applications in stroke. Université d'Ottawa/University of Ottawa; 2023.
  42. Bari E, Ferrarotti I, Torre ML, Corsico AG, Perteghella S. Mesenchymal stem/stromal cell secretome for lung regeneration: the long way through "pharmaceuticalization" for the best formulation. *J Control Release*. 2019;309:11–24.
  43. Singaravelu R, Chen R, Lyn RK, Jones DM, O'Hara S, Rouleau Y, et al. Hepatitis C virus induced up-regulation of microRNA-27: a novel mechanism for hepatic steatosis. *Hepatology*. 2014;59:98–108.
  44. Singaravelu R, O'Hara S, Jones DM, Chen R, Taylor NG, Srinivasan P, et al. MicroRNAs regulate the immunometabolic response to viral infection in the liver. *Nat Chem Biol*. 2015;11:988–93.
  45. Miller S, Krijnse-Locker J. Modification of intracellular membrane structures for virus replication. *Nat Rev Microbiol*. 2008;6:363–74.
  46. Zhang S, Amahong K, Sun X, Lian X, Liu J, Sun H, et al. The miRNA: a small but powerful RNA for COVID-19. *Brief Bioinform*. 2021;22:1137–49.
  47. Yang C-Y, Chen Y-H, Liu P-J, Hu W-C, Lu K-C, Tsai K-W. The emerging role of miRNAs in the pathogenesis of COVID-19: protective effects of nutraceutical polyphenolic compounds against SARS-CoV-2 infection. *Int J Med Sci*. 2022;19:1340.
  48. Mallick B, Ghosh Z, Chakrabarti J. MicroRNome analysis unravels the molecular basis of SARS infection in bronchoalveolar stem cells. *PLoS ONE*. 2009;4:e7837.
  49. Liu Q, Du J, Yu X, Xu J, Huang F, Li X, et al. miRNA-200c-3p is crucial in acute respiratory distress syndrome. *Cell Discov*. 2017;3:1–17.
  50. Tahamtan A, Inchley CS, Marzban M, Tavakoli-Yaraki M, Teymoori-Rad M, Nakstad B, et al. The role of microRNAs in respiratory viral infection: friend or foe? *Rev Med Virol*. 2016;26:389–407.
  51. Pimenta R, Viana NI, Dos Santos GA, Candido P, Guimarães VR, Romão P, et al. MiR-200c-3p expression may be associated with worsening of the clinical course of patients with COVID-19. *Mol Biol Res Commun*. 2021;10:141.
  52. Martinez MA. Compounds with therapeutic potential against novel respiratory 2019 coronavirus. *Antimicrob Agents Chemother*. 2020;64:10–1128.
  53. de Gonzalo-Calvo D, Benítez ID, Pinilla L, Carratalá A, Moncusí-Moix A, Gort-Paniello C, et al. Circulating microRNA profiles predict the severity of COVID-19 in hospitalized patients. *Transl Res*. 2021;236:147–59.
  54. Demiray A, San T, Çalişkan A, Nar R, Aksoy L, Akbubak İH. Serum microRNA signature is capable of predictive and prognostic factor for SARS-CoV-2 virulence. *Turkish J Biochem*. 2021;46:245–53.
  55. Lai-Jiang C, Xu R, Hui-Min Y, Chang Q, Zhong J-C. The ACE2/Apelin signaling, MicroRNAs, and hypertension. *Int J Hypertens*. 2015;2015:1–6.
  56. Wicik Z, Eyileten C, Jakubik D, Simões SN, Martins DC Jr, Pavao R, et al. ACE2 interaction networks in COVID-19: a physiological framework for prediction of outcome in patients with cardiovascular risk factors. *J Clin Med*. 2020;9:3743.
  57. Pierce JB, Simion V, Icli B, Pérez-Cremades D, Cheng HS, Feinberg MW. Computational analysis of targeting SARS-CoV-2, viral entry proteins ACE2 and TMPRSS2, and interferon genes by host microRNAs. *Genes (Basel)*. 2020;11:1354.
  58. Wang Y, Zhu X, Jiang X-M, Guo J, Fu Z, Zhou Z, et al. Decreased inhibition of exosomal miRNAs on SARS-CoV-2 replication underlies poor outcomes in elderly people and diabetic patients. *Sign Transduct Target Ther*. 2021;6:300.
  59. Wang Y-S, Li S-H, Guo J, Mihic A, Wu J, Sun L, et al. Role of miR-145 in cardiac myofibroblast differentiation. *J Mol Cell Cardiol*. 2014;66:94–105.
  60. Wang Y, Li H, Shi Y, Wang S, Xu Y, Li H, et al. miR-143-3p impacts on pulmonary inflammatory factors and cell apoptosis in mice with mycoplasma pneumonia by regulating TLR4/MyD88/NF-κB pathway. *Biosci Rep*. 2020;40(7):BSR20193419.
  61. Matarese A, Gambardella J, Sardu C, Santulli G. miR-98 regulates TMPRSS2 expression in human endothelial cells: key implications for COVID-19. *Biomedicines*. 2020;8:462.
  62. Kaur T, Kapila S, Kapila R, Kumar S, Upadhyay D, Kaur M, et al. Tmprss2 specific miRNAs as promising regulators for SARS-CoV-2 entry checkpoint. *Virus Res*. 2021;294:198275.
  63. Donaldson SH, Hirsh A, Li DC, Holloway G, Chao J, Boucher RC, et al. Regulation of the epithelial sodium channel by serine proteases in human airways. *J Biol Chem*. 2002;277:8338–45.
  64. Stopsack KH, Mucci LA, Antonarakis ES, Nelson PS, Kantoff PW. TMPRSS2 and COVID-19: Serendipity or opportunity for intervention? *Cancer Discov*. 2020;10:779–82.
  65. Bestle D, Heindl MR, Limburg H, Pilgram O, Moulton H, Stein DA, et al. TMPRSS2 and furin are both essential for proteolytic activation of SARS-CoV-2 in human airway cells. *Life Sci Alliance*. 2020. <https://doi.org/10.26508/lsa.202000786>.
  66. Khalaj K, Figueira RL, Antounians L, Lauriti G, Zani A. Systematic review of extracellular vesicle-based treatments for lung injury: are EVs a potential therapy for COVID-19? *J Extracell Vesicles*. 2020;9:1795365.
  67. Leon-Icaza SA, Zeng M, Rosas-Taraco AG. microRNAs in viral acute respiratory infections: immune regulation, biomarkers, therapy, and vaccines. *ExRNA*. 2019;1:1–7.
  68. Sardar R, Satish D, Birla S, Gupta D. Integrative analyses of SARS-CoV-2 genomes from different geographical locations reveal unique features potentially consequential to host-virus interaction, pathogenesis and

- clues for novel therapies. *Heliyon*. 2020. <https://doi.org/10.1016/j.heliyon.2020.e04658>.
69. Rota PA, Oberste MS, Monroe SS, Nix WA, Campagnoli R, Icenogle JP, et al. Characterization of a novel coronavirus associated with severe acute respiratory syndrome. *Science* (80-). 2003;300:1394–9.
70. Trobaugh DW, Klimstra WB. MicroRNA regulation of RNA virus replication and pathogenesis. *Trends Mol Med*. 2017;23:80–93.
71. Calderon-Dominguez M, Trejo-Gutierrez E, González-Rovira A, Beltrán-Camacho L, Rojas-Torres M, Eslava-Alcón S, et al. Serum microRNAs targeting ACE2 and RAB14 genes distinguish asymptomatic from critical COVID-19 patients. *Mol Ther Acids*. 2022;29:76–87.
72. He B, Zhou W, Rui Y, Liu L, Chen B, Su X. MicroRNA-574-5p attenuates acute respiratory distress syndrome by targeting HMGB1. *Am J Respir Cell Mol Biol*. 2021;64:196–207.
73. Parzibut G, Henket M, Moermans C, Struman I, Louis E, Malaise M, et al. A blood exosomal miRNA signature in acute respiratory distress syndrome. *Front Mol Biosci*. 2021;8:640042.
74. Cotroneo CE, Mangano N, Dragani TA, Colombo F. Lung expression of genes putatively involved in SARS-CoV-2 infection is modulated in cis by germline variants. *Eur J Hum Genet*. 2021;29:1019–26.
75. Sung S-Y, Liao C-H, Wu H-P, Hsiao W-C, Wu I-H, Jinpu, et al. Loss of let-7 microRNA upregulates IL-6 in bone marrow-derived mesenchymal stem cells triggering a reactive stromal response to prostate cancer. *PLoS ONE*. 2013;8:e71637.
76. Zipeto D, da Palmeira JF, Argañaraz GA, Argañaraz ER. ACE2/ADAM17/TMPRSS2 interplay may be the main risk factor for COVID-19. *Front Immunol*. 2020;11:576745.
77. Pollard CA, Morran MP, Nestor-Kalinowski AL. The COVID-19 pandemic: a global health crisis. *Physiol Genomics*. American Physiological Society Bethesda; 2020.
78. Xie C, Chen Y, Luo D, Zhuang Z, Jin H, Zhou H, et al. Therapeutic potential of C1632 by inhibition of SARS-CoV-2 replication and viral-induced inflammation through upregulating let-7. *Signal Transduct Target Ther*. 2021;6:84.
79. Gressett TE, Nader D, Robles JP, Buranda T, Kerrigan SW, Bix G. Integrins as therapeutic targets for SARS-CoV-2. *Front Cell Infect Microbiol*. 2022;12:892323.
80. Hynes RO. Integrins: bidirectional, allosteric signaling machines. *Cell*. 2002;110:673–87.
81. Amruta N, Engler-Chiurazzi EB, Murray-Brown IC, Gressett TE, Biose LJ, Chastain WH, et al. In Vivo protection from SARS-CoV-2 infection by ATN-161 in k18-hACE2 transgenic mice. *Life Sci*. 2021;284:119881.
82. Nader D, Fletcher N, Curley GF, Kerrigan SW. SARS-CoV-2 uses major endothelial integrin  $\alpha v \beta 3$  to cause vascular dysregulation in-vitro during COVID-19. *PLoS ONE*. 2021;16:e0253347.
83. Robles JP, Zamora M, Adan-Castro E, Siqueiros-Marquez L, de la Escalera GM, Clapp C. The spike protein of SARS-CoV-2 induces endothelial inflammation through integrin  $\alpha 5 \beta 1$  and NF- $\kappa$ B signaling. *J Biol Chem*. 2022;298:101695.
84. Mortazavi-Jahromi SS, Aslani M. Dysregulated miRNAs network in the critical COVID-19: An important clue for uncontrolled immunothrombosis/thromboinflammation. *Int Immunopharmacol*. 2022;110:109040.
85. Gomes CP, Fernandes DE, Casimiro F, Da Mata GF, Passos MT, Varela P, et al. Cathepsin L in COVID-19: from pharmacological evidences to genetics. *Front Cell Infect Microbiol*. 2020;10:589505.
86. Roa-Vidal N, Rodríguez-Aponte AS, Lasalde-Dominicci JA, Capó-Vélez CM, Delgado-Vélez M. Cholinergic polarization of human macrophages. *Int J Mol Sci*. 2023;24:15732.
87. Liu J, Han X, Zhang T, Tian K, Li Z, Luo F. Reactive oxygen species (ROS) scavenging biomaterials for anti-inflammatory diseases: from mechanism to therapy. *J Hematol Oncol*. 2023;16:116.
88. Hu Y, Guo L, Gao K, Zhang M. Study on the mechanism of Cathepsin L on the activation of M1 macrophages in sepsis-induced acute renal injury. *INDIAN J Pharm Sci*. 2020;82:102–7.
89. Hopkins J, Yadavalli T, Agelidis AM, Shukla D. Host enzymes heparanase and cathepsin L promote herpes simplex virus 2 release from cells. *J Virol Am Soc Microbiol*. 2018;92:10–1128.
90. Geleris J, Sun Y, Platt J, Zucker J, Baldwin M, Hripcsak G, et al. Observational study of hydroxychloroquine in hospitalized patients with Covid-19. *N Engl J Med*. 2020;382:2411–8.
91. Zhao Y, Han M, Xiong Y, Wang L, Fei Y, Shen X, et al. A miRNA-200c/cathepsin L feedback loop determines paclitaxel resistance in human lung cancer A549 cells in vitro through regulating epithelial–mesenchymal transition. *Acta Pharmacol Sin*. 2018;39:1034–47.

## Publisher's Note

Springer Nature remains neutral with regard to jurisdictional claims in published maps and institutional affiliations.